UNCLASSIFIED

AD NUMBER
ADB382358
LIMITATION CHANGES
TO: **Approved for public release; distribution is unlimited.**
FROM: **Distribution authorized to DoD and DoD contractors only; Administrative/Operational Use; JUN 2012. Other requests shall be referred to Naval Air Systems Command, Attn: Code 4.3.1, 48110 Shaw Rd., Patuxent River, MD 20670-1906.**
AUTHORITY
NAWCADPAX errata dtd 2 Jul 2013

THIS PAGE IS UNCLASSIFIED

NAVAL AIR WARFARE CENTER AIRCRAFT DIVISION
PATUXENT RIVER, MARYLAND

TECHNICAL REPORT

REPORT NO: NAWCADPAX/TR-2012/196

CRASH LETHALITY MODEL

by

John A. Ball
Michael Knott
Dr. David Burke

6 June 2012

Distribution authorized to DOD and U.S. DOD contractors only; Administrative or Operational Use; June 2012. Other requests shall be referred to the Naval Air Systems Command (Code 4.3.1), 48110 Shaw Road, Patuxent River, Maryland 20670-1906.

DESTRUCTION NOTICE - Destroy by any method that will prevent disclosure of contents or reconstruction of the document.

DEPARTMENT OF THE NAVY
NAVAL AIR WARFARE CENTER AIRCRAFT DIVISION
PATUXENT RIVER, MARYLAND

NAWCADPAX/TR-2012/196
6 June 2012

CRASH LETHALITY MODEL

by

John A. Ball
Michael Knott
Dr. David Burke

RELEASED BY:

6 Jun 2012
ROLAND COCHRAN / AIR-4.3.1 / DATE
Systems Engineering Division
Naval Air Warfare Center Aircraft Division

REPORT DOCUMENTATION PAGE

Form Approved
OMB No. 0704-0188

Public reporting burden for this collection of information is estimated to average 1 hour per response, including the time for reviewing instructions, searching existing data sources, gathering and maintaining the data needed, and completing and reviewing this collection of information. Send comments regarding this burden estimate or any other aspect of this collection of information, including suggestions for reducing this burden, to Department of Defense, Washington Headquarters Services, Directorate for Information Operations and Reports (0704-0188), 1215 Jefferson Davis Highway, Suite 1204, Arlington, VA 22202-4302. Respondents should be aware that notwithstanding any other provision of law, no person shall be subject to any penalty for failing to comply with a collection of information if it does not display a currently valid OMB control number. **PLEASE DO NOT RETURN YOUR FORM TO THE ABOVE ADDRESS.**

1. REPORT DATE	2. REPORT TYPE	3. DATES COVERED
6 June 2012	Technical Report	May 2011 - February 2012

4. TITLE AND SUBTITLE

Crash Lethality Model

5a. CONTRACT NUMBER

5b. GRANT NUMBER

5c. PROGRAM ELEMENT NUMBER

6. AUTHOR(S)

John A. Ball
Michael Knott
David Burke

5d. PROJECT NUMBER

5e. TASK NUMBER

5f. WORK UNIT NUMBER

7. PERFORMING ORGANIZATION NAME(S) AND ADDRESS(ES)

Naval Air Warfare Center Aircraft Division
48110 Shaw Road
Patuxent River, Maryland 20670-1906

8. PERFORMING ORGANIZATION REPORT NUMBER

NAWCADPAX/TR-2012/196

9. SPONSORING/MONITORING AGENCY NAME(S) AND ADDRESS(ES)

OUSD(AT&L)/S&TS-Unmanned Warfare
Room 3B938
3090 Defense Pentagon
Washington DC 20301-3090

10. SPONSOR/MONITOR'S ACRONYM(S)

11. SPONSOR/MONITOR'S REPORT NUMBER(S)

12. DISTRIBUTION/AVAILABILITY STATEMENT

Distribution authorized to DOD and U.S. DOD contractors only; Administrative or Operational Use; June 2012. Other requests shall be referred to the Naval Air Systems Command (Code 4.3.1), 48110 Shaw Road, Patuxent River, Maryland 20670-1906.

13. SUPPLEMENTARY NOTES

14. ABSTRACT

The purpose of this report is to evaluate the possible modes in which an Unmanned Air System (UAS) could inflict life threatening injuries to 3rd party individuals and develop a model that would calculate the total Lethal Crash Area (LCA) given some standard UAS calculations. A literature search was done to evaluate previous models at determining LCA from aircraft accidents. Two cases were proposed, an inert case in which the individual was impacted by the air vehicle and energetic case where components of the vehicle, namely aviation fuel, reacted to result in a hazardous area around the air vehicle. This report investigated several methods for developing models that could capture both these cases, as well as submodes for each case. An interactive decision making tool, the 3rd Party Risk Assessment Tool was constructed based on the conclusions found in this report. Using the tool, a decision maker may determine the total area related to aircraft parameters can be used to assess 3rd party risk. Ten UAS cases were evaluated and suggest that the factor most correlated to the size of the LCA is the weight of the air vehicle.

15. SUBJECT TERMS

Unmanned Air System (UAS); Lethal Crash Area (LCA); 3rd Party Risk Assessment Tool (3PRAT)

16. SECURITY CLASSIFICATION OF:			17. LIMITATION OF ABSTRACT	18. NUMBER OF PAGES	19a. NAME OF RESPONSIBLE PERSON
a. REPORT	b. ABSTRACT	c. THIS PAGE			19b. TELEPHONE NUMBER (include area code)
Unclassified	Unclassified	Unclassified	SAR	89	Dr. David Burke (301) 342-2185

Standard Form 298 (Rev. 8-98)
Prescribed by ANSI Std. Z39-18

SUMMARY

Expanding the permitted airspace permissions for Unmanned Air Systems (UAS) is a common desire among multiple military and civilian government organizations. Military groups desire to expand the UAS airspace to improve reserve and operational logistics, training exercises, and testing purposes. Civilian agencies, such as police forces, border patrol, and news agencies, would use unmanned air vehicles to conduct aerial surveillance and other missions strongly suited to the UAS. Current air space restrictions limit flight to either restricted airspace, or areas with sparse populations. While lifting these restrictions would have a positive impact on operational envelope and flexibility, due diligence must be used to ensure the public is not subjected to unreasonable hazards.

One of the critical requirements for expanding the operational area of UAS is to understand the risk to uninvolved third parties on the ground posed by the crash of a UAS. In order to address this issue Office of Secretary of Defense, Strategic and Tactical Systems – Unmanned Warfare office, Air Worthiness IPT, has sponsored the Target Level of Safety (TLS) to Third Parties program. The objective of this program is to define a consistent calculation method to determine the relationship between UAS reliability, potential to cause damage, and where it flies. NAVAIR (AIR-4.3.1) has led the effort to develop this methodology. The TLS Program includes five modules: Casualty Expectation, Probability of Loss of Aircraft, Potential Crash Location, Lethal Crash Area (LCA), and Population Density.

This report focuses on the research and development of tools for determining the LCA of a UAS. Prior to analyzing the UAS, one must begin with an examination of the susceptibility of the human body to various injury mechanisms. Through literature research and analysis, a lethal threshold was established and determined to be 54 ft-lb.

With human tolerances defined, the likely LCA of a UAS must be determined. This effort will focus on impacts for four primary modes of aircraft accidents: Fixed Wing Vertical Impact, Fixed Wing Glide Impact, Rotary Wing Vertical Impact, and Rotary Wing Glide or Autorotation Impact. Models were constructed using assumptions gained from literary research, affirmation of physics based equations, and the analysis of actual flight incidents. These models were then built into the 3rd Party Risk Assessment Tool (3PRAT) to verify that the algorithms could produce a reasonably accurate yet simplistic tool for the purposes of determining LCA.

The researchers then examine the effects to which shelter can alleviate some of the dangers to UAS crashes. Shelter calculations were determined by collecting data provided by the Department of Defense (DOD) Explosives Safety Board. The algorithms were compared to three case studies of manned vehicles that impacted different shelters, the resulting fallout, and the accuracy of the model to predict the amount of energy the shelter absorbed during the crash. Finally, standard shelter size and materials were identified for both the rural and urban cases.

The effort of determining the lethal kinetic energy threshold, modeling the different aircraft crash modes to determine the LCA, and determining the effects of shelter may be considered the inert portion of the crash zone. The other aspect of the crash zone is the energetic portion. This is the case where materials on the aircraft, most notably fuel, may cause hazards to personnel as a result of chemical reactions rather than direct impact.

The investigation of energetic sources centered mainly on the analysis of the potential fuel onboard the aircraft. At first, the effects of explosions were examined for the lethal range. This was first done by determining the equivalent weight in TNT of the fuel left in an aircraft's internal fuel tanks. The lethal separation distance due to blast and impulse was then examined by using algorithms developed by the DOD Explosives Safety Board. Similarly, based on the fuel available in the aircraft, the danger to fireballs could be determined. In both cases of blast-impulse and fireball, the size of the lethal area was less than that of the impact area of the vehicle.

A more likely source of injury and lethality to 3rd persons was the effects of primary and secondary fires due to unspent aviation fuel. Using algorithms provided by the Department of Energy, the amount of heat released from a resultant fire in a crash could be determined. This was then correlated with the time it takes human tissue to burn, as well as fatality studies that relate burn amount to lethality. The result for air vehicles that carry large amounts of fuel, the lethal area due to fire induced burns can extend beyond the physical crash site.

For both the inert and energetic models, a decision making tool called the 3PRAT was built. The purpose of this tool is to allow a decision maker to determine the likely lethal crash area based on aircraft parameters. The tool is Excel based to allow ease of transfer of the tool from one individual to another without the associated need for additional support software.

The results of 10 UASs, that are either currently in the U.S. inventory or are being considered for future endeavors, are provided in this report. The LCA for each UAS is calculated for both a gliding and vertical flight termination mode. The aircraft parameter most closely correlated with both LCA due to gliding and vertical descent is the weight of the air vehicle, assumed to be the gross weight. Simply put, heavier vehicles will result in greater crash areas whether it be due to greater potential surface area, more fuel, or the ability of larger wings to carry the vehicle further and faster in the event of a gliding descent.

This report concludes that the principles and scientific assumptions made for the inert portion of flight fatalities is acceptable for inclusion into the 3PRAT decision making tool and may be used to evaluate possible risks associated with UAS flight. Similarly, the affect of secondary fires in the energetic case should also be sufficiently accurate to provide data to the user. The effects of explosions and fireballs were found not to be significant for inclusion into the 3PRAT decision making tool; however, the researchers suggest further investigation be done into these methods before ruling out this lethal mechanism from a complete risk analysis.

Otherwise, the 3PRAT can provide the user helpful information in the decision making process. By delivering a Vehicle Level of Safety, the 3PRAT will calculate the risk of conducting operations of UAS as it relates to 3rd parties on the ground. This information can be used to help decision makers shape mission profiles and configurations to minimize the risk to 3rd parties.

Contents

Page No.

List of Figures

List of Tables

INTRODUCTION

1. A major challenge of integrating Unmanned Aerial Systems (UAS) into the National Airspace System (NAS) is developing a risk-analysis model to quantify the risk to the general public from UAS operations within the NAS. The end goal of risk-assessment analysis is to verify whether a UAS in development can reach a required Target Level of Safety (TLS) defined as one ground fatality per 10 million flight-hours (1 fatality per 10^7 flight-hours) for third parties. In risk-assessment models for aircraft, there are three levels of personnel and the level of risk that they assume. The first are persons flying in the aircraft. These individuals are in the highest danger during a flight termination condition, but have assumed the risks in order to fly on the aircraft. Risk analysis considers these individuals as Level 1. Since the scope of this report will focus on unmanned systems, Level I personnel will not be considered for this analysis. The second set of individuals, Level 2, consists of those who knowingly work or operate around facilities that accommodate aircraft. Examples of these individuals include ground crews and air traffic controllers who have training and knowledge with regard of flight operations. For example, all personnel on a U.S. Navy carrier deck or working on the ramp of an airport are Level 2. This group does not represent the majority of the population within the NAS and are not considered for this analysis. Level 3 or 3rd party individuals consist of those individuals who do not fall into Levels 1 or 2. 3rd party individuals compose the vast majority of the general population who do not work on or around aircraft and are the subject of this research.

LETHAL CRASH AREA

2. The Lethal Crash Area (LCA) for this analysis is defined as the region in which a human lethality would occur during a UAS crash. Initial work in the fields of calculating LCA is based on assumptions of fixed wing geometry. Further research was done to relate the geometric area of a fixed wing UAS coupled with the size of an individual. Ford's *Assessment of the Risk to Ground Population due to an Unmanned Aircraft In-Flight Failure,* provided some guidance on this effort (reference 12). Different flight termination failure modes were examined to include vertical and glide flight termination. Rotary wing geometric models and flight termination modes were also included. These models all made the assumption that within this geometric area, the probability of fatality was equal to one. Further development introduced a kinetic energy relationship with the probability of a fatal injury. A fatal injury is an event that will result in death within 24 hours of the incident without medical attention. This is to eliminate the necessity to evaluate response times to individuals from varying parts of the country. This work continues with the development of a kinetic energy relationship to determine a lethal limit for the typical person exposed to a UAS incident.

3. UAS aircraft present most of the same risks to population as conventional aircraft. These include blunt trauma, blast impulse from fuel air explosion, debris fragmentation, thermal radiation exposure from fire, as well as secondary effects of smoke inhalation and secondary fires. While many of the small scale UAS will not exhibit all of these properties, the larger categories of UAS aircraft currently in service, including Firescout, Reaper, and Global Hawk, will surely represent similar dangers. Dangers not anticipated in UAS flight are related to

systems required for manned flight. Examples of items unique to manned aircraft, which are not explored in this report, are supplemental oxygen systems in the form of liquid oxygen that represent a fire and explosion hazard or, in the case of military aircraft, ejection seats that contain rocket motors that are susceptible to fire.

4. The hazards previously mentioned: air vehicle impact, blast impulse, debris fragmentation, thermal radiation, and secondary fire all have varying degrees of intensity and lethality. The LCA caused by these hazards are determined independently of each other. They are then combined over a Cartesian plan to depict the total hazard area. Areas overlapping different lethality modes are to be considered the union of such regions. Fatalities within these areas are counted once and the effects of lethal modes within the same area are not part of the scope of this research. The first such lethal mode to be investigated is the Kinetic Energy Model.

KINETIC ENERGY MODEL

5. The LCA due to direct impact by the air vehicle is the total area with which an aircraft will come in contact with a person while maintaining enough kinetic energy to cause unrecoverable damage to the body. Due to the complexity of aircraft crashes, it was not possible to construct a complete blunt trauma region for every possible type of crash. Instead, the LCA was approximated for four particular cases; each representing a flight termination mode. The modes are in order of discussion: (1) Fixed Wing Dive/Departure resulting in nose vertical impact with the ground, (2) Fixed Wing glide resulting in belly gliding impact with the ground and skid distance, (3) Rotary wing unrecoverable loss of main rotor(s) rotations per minute (RPM) resulting in belly vertical impact with the ground, and (4) Rotary wing autorotation resulting in belly landing with ground.

6. In order to calculate the air vehicle impact area, the lethal limits on the human body must be known. This report begins with Burke's previous work to develop a System Level Airworthiness Tool (SLAT) (reference 6) and attempts to construct a deeper more empirical approach in determining the kinetic energy limit to an individual for the purpose of determining LCA.

REFERENCE MAN

7. The first step in developing a kinetic energy threshold is identifying a representative model for 3rd party individuals. Some assumptions must be made regarding the size, shape, and weight of a representative human model. In a paper presented by Janser regarding lethality due to debris and fragments, Figure 1 was given as the geometry of the reference person (reference 18).

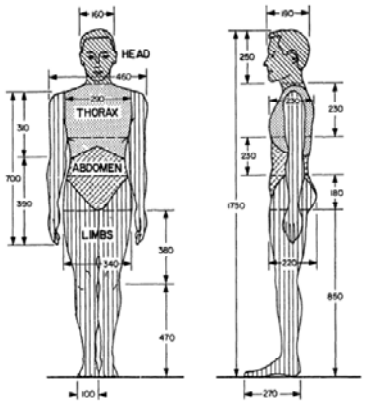

Figure 1: Standard Reference Man

8. Likewise, the International Commission on Radiological Protection provides the following description: "Reference man is defined as being between 20-30 years of age, weighing 70 kg, is 170 cm in height, and lives in a climate with an average temperature of from 10° to 20°C" (reference 16). It should be noted that these definitions were created 30 years ago and may no longer represent the population in question. Therefore, the 95th percentile American male ages 20-30 as defined by the National Aeronautics and Space Administration (NASA) in 2000 will be used for this analysis (reference 29). Using the 95th percentile American male provides the largest and most conservative susceptible volume that could be impacted by an UAS. NASA defines the 95th Percentile man as 190.1 cm tall with a waist back of 51.6 cm and weighs 98.5 kg. Figure 2 shows a diagram of the NASA 95th percentile American male.

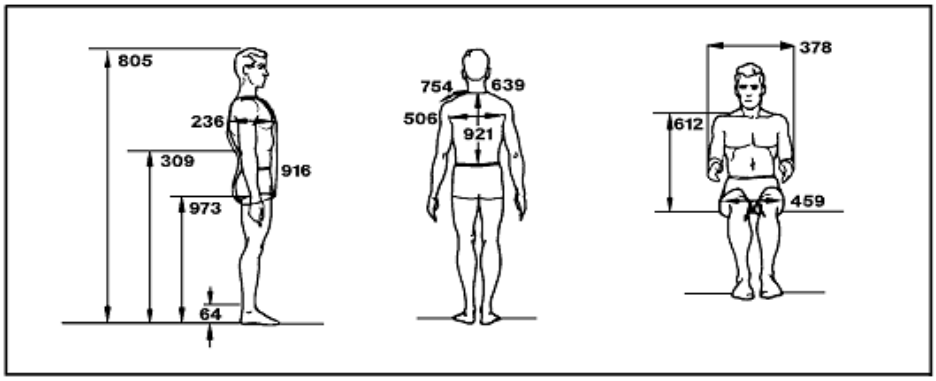

Figure 2: Geometry of the 95th Male as defined by NASA

9. Anthropometric diagrams such as those in Figures 1 and 2 display the great variation in organ susceptibility between the different regions of the body. This makes it difficult to give a detailed and accurate model. For the purposes of this effort, an approximate model separating the head, torso, and limbs will be implemented. This reference man approximation model used in this report can be seen in Table 1.

Table 1: Reference Man Approximation

Weight		Height		Diameter	
70	kg	1.9	m	46	cm
154.3235834	lb	6.23	ft	1.5	ft
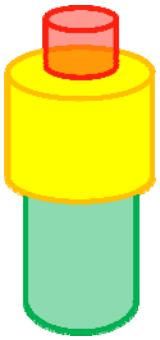		Sub-Parts			
		Head			
		Height		Diameter	
		26.7	cm	16.5	cm
		10.51	in.	6.50	in.
		Thorax/Abdomen			
		Height		Diameter	
		70	cm	46	cm
		27.56	in.	18.11	in.
		Limbs			
		Height		Diameter	
		93.3	cm	42.3	cm
		36.73	in.	16.65	in.

10. Research into the susceptibility of each of these regions was conducted. The results for the Head, Thorax/Abdomen, and Limbs are provided in the following paragraphs.

HEAD AREA – SKULL FRACTURE

11. The head represents a small overall volume and mass percentage of the human body, however, the location of several key organs (cortex, brain stem, throat, nasal cavity, etc.) makes this region vulnerable to impacts. One means of determining the severity of a head impact is to observe the amount of skull fracture that occurs. A particular head may exhibit significant skull fracture, yet if the impact failed to cause enough intracranial damage to be fatal the victim may survive. Similarly, lethal impacts to the head can result without causing any skull fracture. Research was unable to find a positive study correlating skull fracture to lethality, however, one study was found that suggests a correlation of lethal head injury to skull fracture. A recent medical study on fatal head injuries of road collisions in Nepal determined that 85.7% of fatal head injuries showed signs of skull fracture and over half of those contained fractures at the base of the skull (reference 19). For the purposes of this effort, the assumption is made that skull fracture, particularly fractures to the base of the skull, result in a fatal head injury when left untreated for 24 hours.

12. Literature searches revealed a useful model that connected the probability of skull fracture to Kinetic Energy. To calculate the threshold value used for this study, a term relating several factors of skull fracture is introduced. Blunt Criteria (BC) is a measure of the susceptibility of the skull to fracture as a function of kinetic energy, the mass of the skull, the combined thickness of

skull and soft tissue, and the diameter of the object striking the skull. The equation for BC is provided as follows:

$$BC = LN\left(\frac{KE}{m_{skull}^{1/3} \times T \times D}\right) \qquad (1)$$

Where:
KE = Kinetic energy in Joules
m_{skull} = mass of skull in KG
T = Thickness of skull and soft tissue
D = Diameter of projectile in cm

13. Raymond et al, conducted kinematic tests on cadaver skull (reference 34). The diameter of the study's projectiles was 38.1 mm. The average skull thickness was measured to be approximately 4.8 mm and the soft tissue as 8.1 mm. Using regression analysis, Raymond et al developed a logistic function curve of the form:

$$P_{Skull\ Fracture} = \frac{1}{1+e^{(-\alpha-\beta \times BC)}} \qquad (2)$$

Where:
$P_{skull\ fracture}$ = Probability of skull fracture.
BC = Blunt Criteria
α = β = Constants

14. Where α and β were determined based on test results. The curve that related the BC value to the probability of skull fracture resulted in a tight confidence interval and a two tailed statistical p-value below at 0.05. The plot is provided below for α equal to -5.818 and β equal to 3.605 based on the test results (Figure 3).

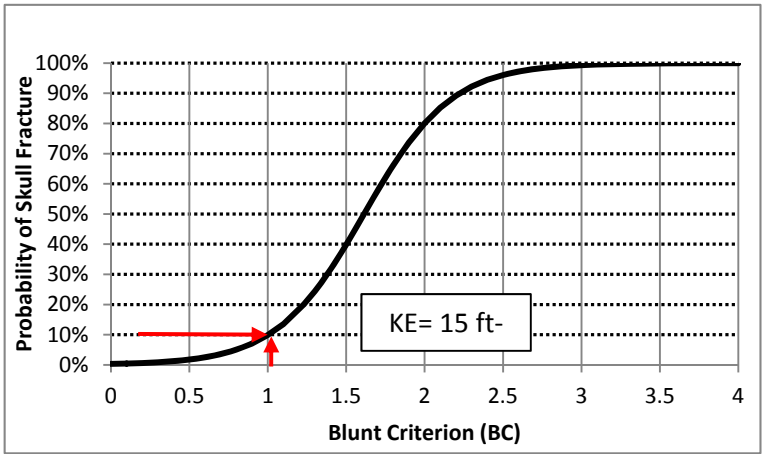

Figure 3: Probability of Skull Fracture and Lethal Kinetic Energy Threshold

15. A probability of skull fracture of 10% was selected as the lethal limit. It was decided that below this value may result in too conservative a result, while any higher would not be sufficient to capture the lethality due to skull fracture. From the plot, one can see that a probability of 10%

skull fracture corresponds to a BC value of 1.0. Solving for the kinetic energy of lethality using equation 1 yields equation 3. By using equation 3, the threshold kinetic energy of 15 ft-lb was found. This kinetic energy is that of which one would expect a 10% probability of skull fracture.

$$KE = e^{BC_{Lethal\,Percent}} \times m_{skull}{}^{1/3} \times T \times D \qquad (3)$$

Where:
KE = Kinetic energy
BC = Blunt Criteria
m_{skull} = Mass of skull
T = Thickness of skull and soft tissue
D = Diameter of the projectile

16. It should be noted that the average age of the specimens for the study was 67 years. Zhou provided a review of age effects on the tensile strength of human cortical bone and found that maximum strength occurred between 30 and 39 years (reference 39). Ultimate strength decreased by 15–25% for the age group of 70–80 years. Therefore, fracture thresholds derived from the current study and the referenced studies should be considered as conservative estimates for skull fracture tolerance of the 20-30 year old reference man.

17. In summary, the following assumptions are made to calculate the lethal 15 ft-lb of kinetic energy required to cause lethality due to head impact:

- It was assumed that skull fracture, particularly to the base of the skull, results in lethality without treatment over a 24 hour period.
- It was determined that a 10% risk of skull fracture was the limit in which to be evaluated.
- The average skull and soft tissue thickness represents the averages for the general population.
- It is also assumed that the skull has uniform thickness and strength.
- The studies conducted have been done on cadavers of an average age of 67. The values collected would be considered a worst case scenario.

THORAX/ABDOMINAL AREA – BLUNT TRAUMA

18. The second major area of concern is the thoracic and abdominal regions. Previous work went into the development of SLAT as an evidence-based approach to evaluating small UAS airworthiness (reference 6). The SLAT method examined the effects of non-penetrating missiles. For penetrating missiles, lethality occurs due to essential organ failure. The extent of missile penetration as a function of shear forces reacting along the target with the projectile. Different essential organs in the body all have different susceptibilities to these penetrating missiles. Due to the complexity of internal organ failure from penetrating projectiles, this work follows the methods proposed in SLAT of non-penetrating missiles. This was felt to limit the scope of the lethality threshold with respect to time and complexity.

19. Lethality thresholds in other works were either over conservative, such as the analyst assuming that the entire body had the same lethal limit as the head, or the kinetic energy value was selected arbitrarily such as the NATO kinetic energy threshold of 58 ft-lb[1]. Instead, the kinetic energy lethality threshold used in SLAT was determined to be 49 ft-lb of energy. This lethality threshold was determined by investigating a technical report by the Army Research Laboratory (reference 24). The report attempted to assemble and correlate blunt trauma data with primary emphasis on the relevancy of the data for soft body-armor. The methodology used in the experiments involved the use of dogs and goats with impacts to the thoracic region.

20. This report used the source data of the Army Research Laboratory (reference 24) report that was published in previous studies on lethality by Bowen (reference 5) and Clare (reference 8). Bowen and Clare sought to identify lethal blunt trauma kinetic energy levels for the purpose of modeling the risk to people. This was in support of the department of energy and the nuclear energy commission who were concerned for civilian casualties during a nuclear conflict. Animals would be sedated, strapped down, and hit with calibrated cylinder projectiles.

21. Closer examinations of these tests revealed that the testing included canine, goat, and swine animal tests in their results. Due to the mass of the swine test subjects being significantly less than the goat and canine data, it was felt that the swine results should not be combined with the goat and canine data. The results of the animal tests would eventually need to be scaled to a human sized mass and, therefore, it was felt the swine test used in the experiments were not acceptable to scale to human proportions. This report rejected the swine data in favor of the animal test subjects with higher mass.

22. From analysis of the animal data, it is possible to construct a probability of lethality curve fit based on the ratio of kinetic energy to the product of projectile diameter and target weight. The animal lethality data were entered into MATLAB© and the function cftool() was used to generate a logistic function. The x-axis represents a ratio of kinetic energy to the product of projectile diameter and target weight as defined by equation 4.

$$x = LN\left(\frac{0.5MV^2}{WD}\right) \qquad (4)$$

Where:
M = Mass of Projectile
V = Velocity of the projectile
W = Weight (mass) of the target
D = Diameter of the projectile

23. Once the ratio of kinetic energy to weight and diameter of the projectile was determined, the probability of animal death was determined for each data point. It is important to note that modeling lethality was difficult because the severity of injuries in the study were binomial. That is, each test run resulted in only lethal or non-lethal events. For this effort, the definition of lethality was based on injuries sustained to cause mortality within 24 hours without medical care.

[1]The 58 ft-lb (76 J) can be traced to an early 20th century German officer. There appears to be no research in the literature as to the methods used to select this value.

The data, however, is based on animal experiments where survivors of projectile impact were "humanely" put down if they had not succumbed to their injuries within an hour. Still, the animal data is the best source of information in regards to blunt trauma and lethal limits and was used for the scope of this report (Figure 4).

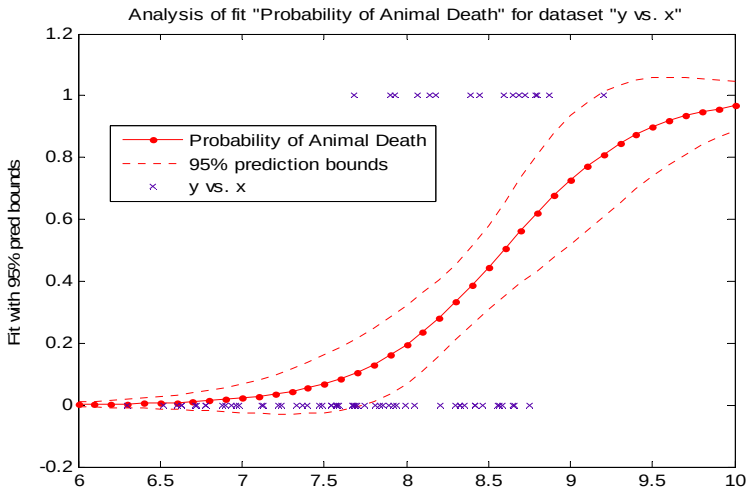

Figure 4: Analysis of the Probability of Animal Death

24. The logistics function used in Figure 4 defining the probability of animal death is shown in equation 5. The values of α and β were determined to be -2.395 and 20.58, respectively.

$$P_{Blunt\ Trauma} = \frac{1}{1+e^{(\alpha X+\beta)}} \qquad (5)$$

Where:

$P_{Blunt\ Trauma}$ = Probability of death as a result of blunt trauma
X = Ratio of kinetic energy to product of objects weight and diameter
α = β = Constants

25. There is confidence that a lethal probability of 10% threshold value can be used. Figure 5 shows the results of the animal data, the logistic function model, and the 10% threshold. The threshold happens to correspond to the lowest ratio of which an animal passed away. By using equations 4 and 5 and solving for kinetic energy based on the animal testing data, a kinetic energy of 56 ft-lb was found. This information is only valid for thorax blunt impacts, however, for simplicity, an additional assumption is made that the abdomen and thorax have the same susceptibility of lethality such that the entire middle region can be modeled the same. Given the thoracic region is more susceptible to blunt trauma than the abdomen; this was considered a conservative and appropriate assumption.

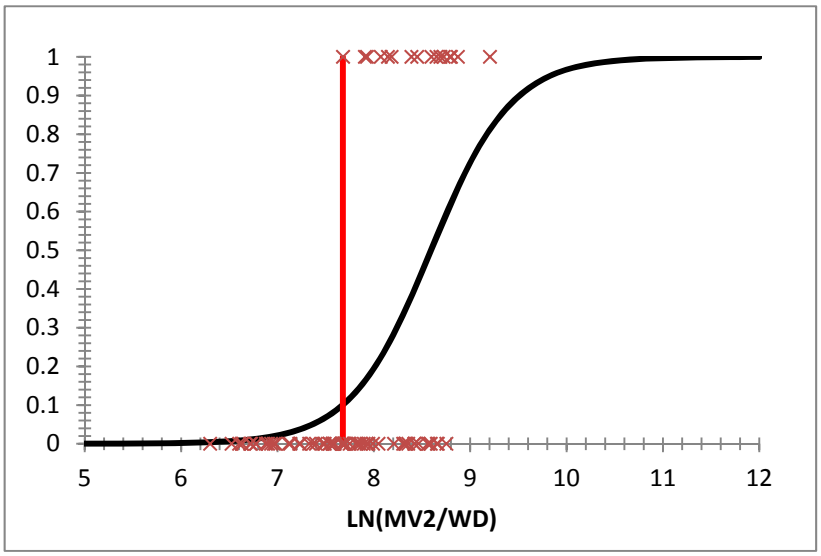

Figure 5: Blunt Trauma Lethality Analysis

26. Because the threshold value presented in this report was determined from animal data, there was a desire to validate the results. The kinetic energy analysis of common spherical objects was repeated with the updated model using probabilities of lethality. The results are provided in Table 2 to make the values more common to decision makers.

Table 2: Velocity as a Function of Probability of Lethal Impact

	Velocity (mph) at Probability of Lethal Strike				
Projectile Name	10%	20%	50%	90%	95%
BB	1396	1649	2204	3488	4060
Bean Bag	62	73	98	155	181
Golf Ball	128	152	203	321	374
Baseball	72	85	114	180	210
Bowling Ball	19	23	31	49	57
	Kinetic Energy (ft-lb)				
BB	56	78	139	349	473
Bean Bag					
Golf Ball					
Baseball					
Bowling Ball					

27. Note the very high velocity of the BB. Due to the small size and relatively high density, the BB will impact with shear force strong enough to penetrate tissue at lower velocities than given here. As previously stated, this analysis assumes no penetration. The value given is just the effective velocity required to achieve specific blunt traumas assuming no penetration.

28. The remaining objects and velocities to the casual observer seem reasonable to be able to cause life threatening injuries. In fact, there have been reports of individuals struck in the thorax from baseballs that have caused death both in professional as well as in adolescents where speeds of baseballs were lower than posted above. As a result, there is confidence in the kinetic energy threshold value of 56 ft-lb.

29. In summary, the following assumptions are made to determine the abdomen/thorax kinetic energy threshold of 56 ft-lb:

- Blunt trauma was used to conduct all analysis. The projectiles were not capable of penetrating the person.
- Lethal injuries due to blunt trauma are those injuries resulting in lethality without treatment over a 24-hr period.
- The abdomen and thorax have the same susceptibility to impacts.
- Lethality results are based on animal tests of canine and goats, but swine tests used in previous efforts were rejected due to the test subjects' smaller relative mass

LOWER LIMBS – BLUNT TRAUMA (ASSUMED)

30. Given the lack of information regarding the risk of lethality due to limb impact, the lower limb section is assumed to have the same risk as that of the thorax/abdominal region only the cylinder is taller and narrower.

COMBINED RESULTS

31. A simplified kinetic energy model was desired that could combine the effects of both blunt trauma to the thorax and abdomen, and skull fracture. To incorporate the two fundamentally different lethal mechanisms, a weighted average of lethal energy was used based on the volume of the body parts. Using the simplified man from Table 1, the volume weighted lethal kinetic energy is calculated using equation 6 where V is volume in cubic inches.

$$KE_{avg|Lethality} = \frac{(V_{Head} \times 15\ ftlb) + (V_{Torso} + V_{Limbs}) \times 56 ftlb}{V_{Head} + V_{Torso} + V_{Limbs}} \qquad (6)$$

The result is a weighted average kinetic energy threshold of 54 ft-lb. It may interest the reader to know that this value, determined through empirical analysis of animal and cadaver testing, is relatively close to the 49 ft-lb suggested by Burke for implementation into the SLAT tool (reference 6) and the 56 ft-lb published by NATO. Based on the empirical evidence and the relative agreement of this kinetic energy threshold to previously published values, 54 ft-lb is an acceptable kinetic energy limit for the purposes of determining LCA due to air vehicle impact.

AIRCRAFT CRASH MODELS

32. Several researchers have proposed different methods for modeling the size and severity of UAS crashes. Most models depend on aircraft geometry with only a few exhibiting higher fidelity to consider factors such as impact velocity. The models for fixed wing aircraft were derived from this previous research, but were modified with the goal improving the fidelity of the models. The aircraft models include Fixed Wing Dive, Fixed Wing Glide, Rotary Wing Dive, and Rotary Wing Glide. For all of the following models, it is assumed that the aircraft remains intact until impact with the ground (e.g., no mid-air breakup).

FIXED WING DIVE

33. The first aircraft crash model describes the flight termination of a fixed wing aircraft and subsequent vertical descent also known as Fixed Wing Dive. Figure 6 provides a schematic of this scenario.

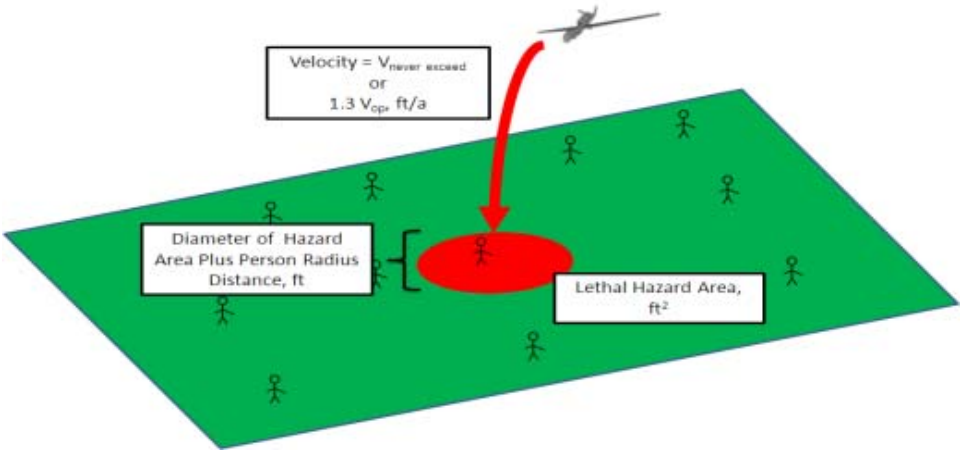

Figure 6: Fixed Wing Dive Description

34. Previous work (reference 2) suggests that a vertical flight termination for fixed wing aircraft results in an Impact Area (IA) of:

$$IA_{vert\ FW} = \pi \times \left(\frac{1}{2} \times b_{aircraft} + R_{person}\right)^2 \qquad (7)$$

Where:
IA = Impact Area
B = Wing Span of Aircraft
R = The radius of the 95th percentile male.

35. From equation 7, one can see that the case of the vertical aircraft IA is approximated as a circle with radius of half the wingspan plus the radius of the average person. This value is used to approximate the total probable area of which a person could be impacted. Other means of

determining pure vertical failure mode are available, however, it was felt this conservative approximation allows determination of area dependent on one early design factor, wingspan. Given that aircraft may impact the ground in multiple types of geometries (ex., Nose first, tail first, belly spin) the wingspan impact area is a good approximation of worst case scenario given that most fixed wing UASs in operation (and all used later in this report) have wingspan as their largest dimension.

36. The radius of the person is not the distance of an individual to the impact center. It is the radius of the 95th percentile American male. This is added to the wingspan to indicate the combined radius of a circle where someone could be struck. This relationship is shown in Figure 7.

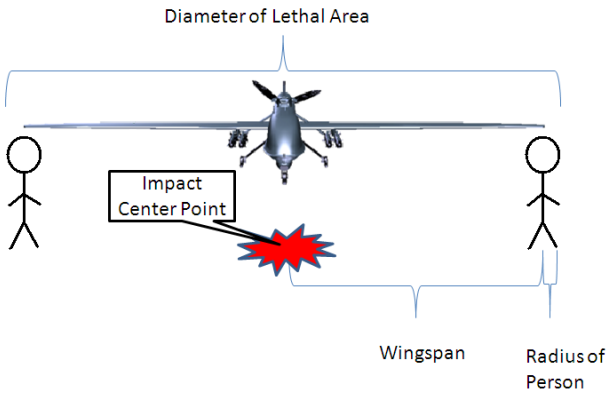

Figure 7: Diameter of Lethal Area

37. The determination of the kinetic energy of a crash must be done using a velocity pertinent to the type of failure. The velocity of the airframe is critical in determining the kinetic energy. However, knowing the actual velocity at the time of impact is difficult to achieve. For simplification purposes, the velocity chosen to be used is the never exceed velocity, V_{ne}. This velocity is typically determined early in the design process and reflects the maximum speed an aircraft is designed to withstand before aerodynamic loads cause catastrophic failure of the structure of the airframe. Using V_{ne}, the equation for kinetic energy is given as equation 8.

$$KE_{vert\ FW} = \frac{1}{2} \times \frac{GW_{lbs}}{32.2\ ft/s^2} \times \left(1.68780986 \frac{ft/s}{kts} \times V_{ne}\right)^2 \qquad (8)$$

Where:

$KE_{vert\ FW}$ = Kinetic Energy of Aircraft
GW = Gross Weight of the aircraft
V_{ne} = Never Exceed Speed of the aircraft.

38. It is important to note that the velocity is in true airspeed. For this and all subsequent models, effects of wind are assumed negligible.

39. In summary, the impact area is determined solely as a function of the wingspan. The corresponding kinetic energy is dependent on the gross weight (GW) and the velocity limit of the

air vehicle. Finally, when using this model one must be aware of the assumptions previously stated:

- •Effects of winds are negligible.
- •The max speed of the airframe in a vertical descent is the never exceed airspeed, V_{ne}.

FIXED WING GLIDE

40. The second impact model describes the impact of a fixed wing aircraft impacting the ground in a horizontal configuration. The total impact area from a gliding UAS must represent both the glide area with which a UAS could strike an individual and the subsequent area the vehicle covers as it skids along the surface of the ground. Figure 8 shows the possible impact area for glide descent.

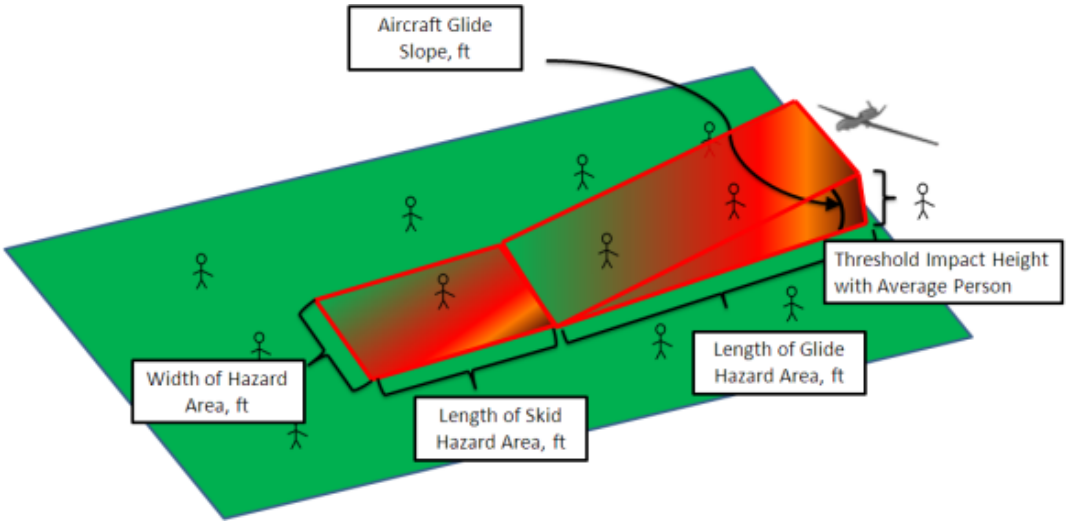

Figure 8: Fixed Wing Glide Description

41. Similar to the fixed wing dive approach and following the efforts of Reece Clothier, the width of the hazard area is defined as the aircrafts wingspan ($b_{aircraft}$) plus a buffer distance of the radius of a person (R_{person}) on both sides of the aircraft (reference 9). This relationship can be seen in equation 9.

$$W_{Haz} = b_{aircraft} + (2R_{Person}) \qquad (9)$$

42. Equation 9 gives the width of the potential strike area. The length of this hazard area is broken into two sections, the glide distance and the skid distance. The glide distance is defined as the distance the aircraft glides from a height of the 95th percentile American male until it makes contact with the ground. The skid distance is defined as the distance the aircraft travels after it impacts the ground until it loses enough kinetic energy as to cause a non-lethal impact with

potential bystanders. Both the glide and skid distance of an aircraft are going to vary with each aircraft. These lengths are discussed in detail in the following paragraphs.

Glide Hazard Length

43. From Figure 8, it can be seen that the glide distance can be determined based on the threshold height at which a person could be struck and the glide angle of the air vehicle. Using equations developed by Anderson, the length of the glide distance (L_{Glide}) can be computed as a function of the height of the person (H_{95th}) and the glide angle (γ) of the UAS (reference 1). This relationship can be seen in equation 10.

$$L_{Glide} = \frac{H_{95th}}{tan\,(\gamma)} \qquad (10)$$

44. The height of the individual is the height of the 95th percentile American male. Two methods for determining the glide path angle were evaluated. The first method is a Table provided by the Department of Energy (DOE) Standard *Accident Analysis for Aircraft Crash into Hazardous Facilities* (DOE-STD-3014) and the second method is done by evaluating the aerodynamic performance of the air vehicle (reference 38).

45. The first method for determining glide slope is by referencing the data collected for the DOE-STD-3014. Information from Table 3 developed by the DOE for accident analysis of aircraft crashes into hazardous facilities, DOE-STD-3014.

Table 3: Mean Aircraft Impact Angle

Aircraft Category	Commercial Aviation	General Aviation	Helicopters	Military Aviation			
				Large Aircraft		Small Aircraft	
				Takeoff	Landing	Takeoff	Landing
Mean (COT(γ))	10.2	8.2	0.58	7.4	9.7	8.4	10.4
γ; deg	5.60	7.0	60	7.7	5.9	6.8	5.49

46. The following assumptions must be kept in mind when calculating the overall length of the glide slope based on the values provided in Table 3:

- The numbers given are averages determined by the DOE.

47. The information contained within the DOE-STD-3014, was derived from data collected from National Transportation Safety Board (NTSB) reports and military safety centers.[2] Should information regarding the general characteristics of the aircraft be unavailable or the methods described in the following section are not applicable, Table 3 may be used. This method does not provide the capability to adjust values based on unique aircraft characteristics. If more information is available, the following model may be used to calculate glide slope.

[2]Greater detail into the DOE-STD-3014 sources is discussed in the Skid Hazard Length section.

48. When the maximum lift to drag ratio for an aircraft is known, the glide angle can be determined precisely and as a result so can the hazard strike area. The minimum glide angle descent can be calculated using equation 11 as provided by Anderson (reference 1). This minimum glide angle will correspond to the maximum hazard area of which an aircraft still airborne could strike a person. By taking equation 11 and substituting it into equation 10, it is possible to determine the length of the strike area very accurately. This can be seen in equation 12.

$$\tan(\gamma)_{min} = \frac{1}{(L/D_{max})} \qquad (11)$$

$$L_{Glide} = \frac{H_{95th}}{tan\,(\gamma)} = \frac{H_{95th}}{\frac{1}{(L/Dmax)}} = H_{95th} * \left(\frac{L}{D}\right)_{max} \qquad (12)$$

49. In the case that the maximum lift to drag ratios are not know, it may be possible to estimate the gliding impact area based on a parametric relationship established below (reference 33). The aircraft impact areas are plotted in Figure 9 according to their respective wingspan.

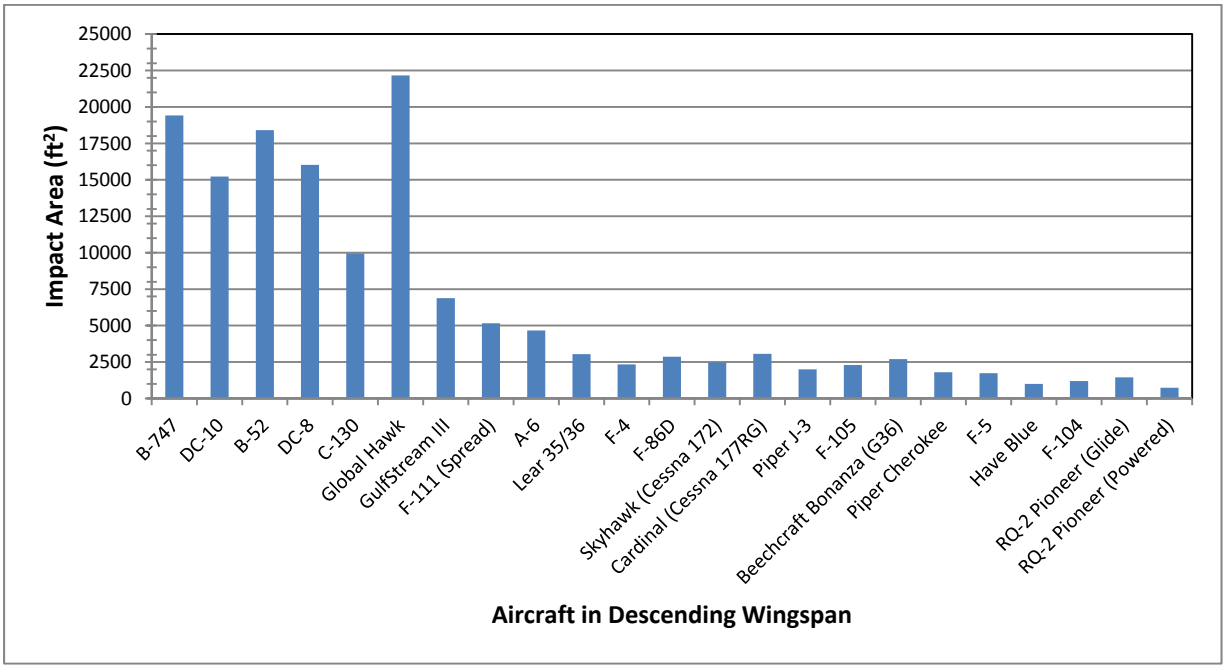

Figure 9: Aircraft Impact Area of Varying Aircraft

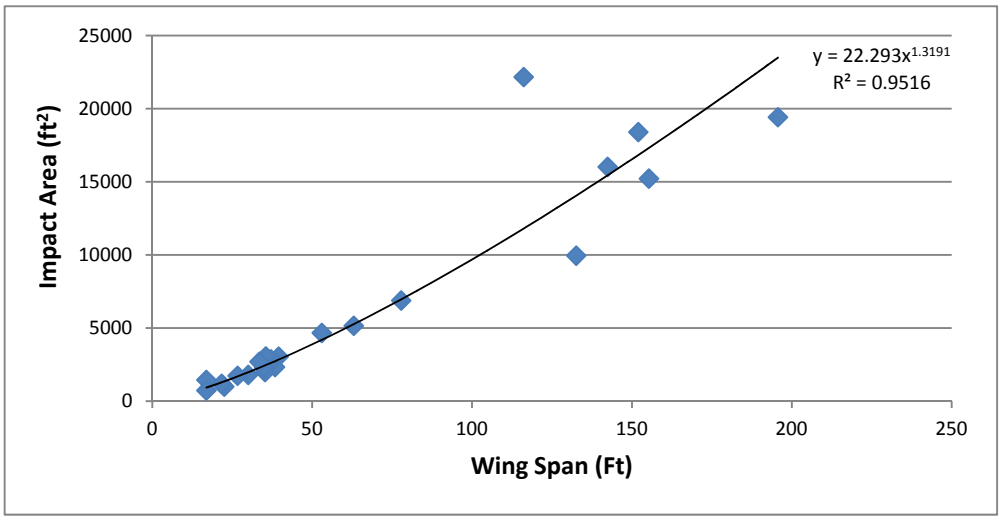

Figure 10: Impact Area with Respect to Wing Span

50. As can be seen in Figure 10, the wingspan relationship has a strong relationship to overall impact area. Due to this relationship, it is proposed that for determining the overall glide impact area, the following equation be used.

$$IA_{Glide} = 22.293\ \mathrm{b}^{1.3191} \qquad (13)$$

Where:

IA_{Glide} = Gliding impact area

b = aircraft wingspan

51. This method provides a simple means of calculating the overall impact area, and is based on parametric results of a database of both manned and unmanned aircraft. It should be noted that this analysis is best for aircraft that have conventional configurations. Unique aircraft configurations, such as the Global Hawk UAS, will not conform perfectly to this result due to the disproportionally long wingspan. In the case of outliers, it is better to find the glide path via the maximum lift to drag ratio.

52. For determining the length of the glide area, it is ideal to use the maximum lift to drag ratio when known to give the most accurate results. When the maximum L/D is not known, use the equation that relates total glide impact area based on wingspan to provide a result based on parametric data. Finally, should no other amplifying information be available, the DOE-STD-3014 may be used to determine the glide path angle and the subsequent impact distance calculated from the tabulated results. While Anderson and others have provided means for estimating the glide distance, the estimation of skid distance was found to be less defined.

Skid Hazard Length

53. When an aircraft impacts the ground in a gliding manner, it will tend to slide or skid some distance. The authors of this report could not find any previous effort to model the skid distance of an aircraft following impact with the ground, however, previous research suggests aircraft skidding is a significant portion of the total crash area.

54. This report proposes two methods for determining fixed wing skid distance. The first is a basic rigid body dynamics model making several assumptions while the second is based on data collected from aircraft incidents.

55. The first method assumes simplified rigid body dynamics in straight line motion. This suggests that the aircraft remains intact upon impact with the ground and maintains straight line motion. This is a conservative assumption since aircraft breakup during the skid will consume energy. In addition, if there is any deviation from the straight line skid, there will be an overall shorter skid length. Once impacting the ground this method assumes that aerodynamic drag forces are negligible. The assumption here is that the drag forces exhibited by the terrain to the air vehicle will be orders of magnitude greater than that of air resistance. Given these assumptions, the skid distance could be determined from equation 14.

$$L_{Skid\ Lethal} = \left(V_{Glide} t_{safe}\right) - \left(\mu_{slide} g t_{safe}^2\right) \qquad (14)$$

Where:

$L_{Skid\ Lethal}$ = Lethal skid length
V_{glide} = Horizontal component of aircraft velocity
μ_{slide} = Coefficient of friction between terrain and aircraft
g = Gravitational constant
t_{safe} = Time required to slow the aircraft to a safe strike speed

56. As previously stated, t_{safe} represents the time required for the aircraft to slow down to a velocity where the kinetic energy is no longer lethal. While the air vehicle may skid further, at some point in the skid it no longer poses a hazard to individuals due some point in the skid it no longer poses a hazard to individuals due to impact.[3] This time can be determined from equation 15.

$$t_{safe} = \frac{V_{Glide} - V_{Min\ Kill}}{2 \times \mu_{slide} \times g} \qquad (15)$$

Where:

t_{safe} = Time required to slow the aircraft to a safe strike speed
V_{glide} = Horizontal component of aircraft velocity
$V_{min\ Kill}$= Minimum lethal velocity of aircraft as defined by equation 16
μ_{slide}= Coefficient of friction between terrain and aircraft
g = Gravitational constant

[3]The authors recognize that for heavy aircraft with larger momentums, the difference between the lethal skid distance and the total skid distance would be negligible. This term is out of consideration for current smaller and lighter UAS.

$$V_{Min\ Kill} = \sqrt{2 \times \frac{W_{lbs}}{g} \times KE_{Lethal}} \qquad (16)$$

Where:

$V_{min\ kill}$ = Minimum lethal velocity of aircraft
W_{lb}= Weight of the aircraft in pounds
g = Gravitational constant
KE_{lethal} = Lethal Kinetic Energy previously determine to be 54 ft-lb of energy

57. For the above equations, if an appropriate coefficient of friction can be assumed between terrain composition and aircraft manufacturing material, only the velocity at impact with the ground should be needed to determine the lethal skid length. An issue with this assumption is that researchers of this report could not find coefficients of friction between soil and typical aircraft skin materials such as aluminum and that these coefficients would be generalized and not likely represent the effects of the vehicle.

58. Due to the lack of information regarding the coefficient of friction between an aircraft and various terrains, a second method of determining the skid hazard length is proposed. Using data for manned incidents, a parametric model could be built. The initial investigation for such as source was found in the DOE-STD-3014. This can be seen in Table 4.

Table 4: Aircraft Mean Skid Distances

Aircraft Category	Commercial Aviation	General Aviation	Helicopters	Military Aviation			
				Large Aircraft		Small Aircraft	
				Takeoff	Landing	Takeoff	Landing
Mean Skid Distance (ft)	1,440	60	0	780	368	246	447

59. Further examination of these values would reveal that the distances provided in the standard do not necessarily match with the work done in the source documentation. The basis of the DOE-STD-3014 is the *Data Development Technical Support Document for the Aircraft Crash Risk Analysis Methodology (ACRAM) Standard* (reference 21). Values within the ACRAM report do not match with the findings of the DOE-STD-3014. Therefore, a further analysis was done into the ACRAM documentation to ensure that reasonable skid distance values could be found for the purposes of UAS crashes.

Fixed Wing Skid Distance: Military Aircraft

60. Military aircraft often have unique performance requirements and capabilities in order to accomplish required strategic and tactical goals. The skid distances provided in the ACRAM study were originally based on data from the Minuteman III Weapon System Safety Assessment (WSSA) database. According to the ACRAM study, these military events were only applicable to instances not near an airfield, as the original study for the Minuteman III WSSA database was concerned about aircraft crashing into missile silos. Therefore, this information should be considered consistent with the overall approach of this report for determining the risk to 3rd party

individuals. One of the observations made with the data was that aircraft landing at greater that 20 deg glide path resulted in zero skid distance (only crater and subsequent debris). In instances where the skid distance was not zero, aircraft skid distances were comparable to their respective classes. Table 5 provides the skid distance cumulative probability distributions provided by the ACRAM study for military aircraft in both the takeoff and landing configurations for both small and large aircraft (reference 21)[4,5].

Table 5: Skid Distance Distribution for Military Aircraft

Skid Distance				
	Large Aircraft		Small Aircraft	
Cumulative Probability	Landing	Takeoff	Landing	Takeoff
40%	0	0	0	0
45%	0	0	131	0
50%	0	0	200	0
55%	185	0	262	0
60%	262	1326	326	0
65%	335	1498	396	125
70%	414	1568	477	242
75%	505	1717	574	330
80%	617	1817	698	431
85%	768	1925	868	560
90%	999	2056	1142	752
95%	1461	2245	1740	1134
100%	∞	∞	∞	∞

61. For the fixed wing UAS case, a UAS powered with a turbojet or turbofan engine will be classified as a "Small Military Aircraft" for the purposes of determining the skid distance. Propeller driven UAS, even those with turboprop engines, will be considered as general aviation and will be discussed in a later section.

62. The DOE-STD-3014 did not identify the assumptions, conclusions, or discuss the process by which the mean skid distances for military aircraft were selected. To compare the DOE-STD-3014 results to that document's source, the ACRAM study[6], Figure 11 shows the cumulative probability results from Table 5 with the mean skid distances concluded in the DOE-STD-3014.

[4]Some clarification must be done for these aircraft types. Large aircraft are to be considered bomber or cargo aircraft and data are extracted from the following aircraft: B-1, B-2, B-52, C-5, C-9, KC-10, C-12, C-130, KC-135, and C-141.

[5]Small aircraft are considered as "performance" aircraft such as attack, fighter, and training aircraft with a database of aircraft including: A-7, A-10, A-37, F-4, F-5, F-15, F-16, F-106, F-111, F-117, T-33, T-37, T-38, T-39, and T-41. With the exception of the T-41, all the small aircraft are non-propeller equipped aircraft.

[6]The Minuteman III WSSB database was unavailable for validation of the ACRAM results; however, the assumption is correct.

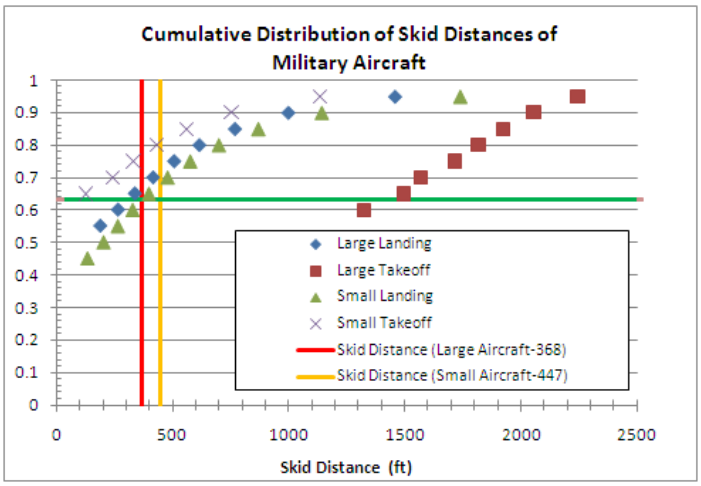

Figure 11: Mean Skid Distance and Probability of Skid for Military Aircraft

63. Figure 11 plots show each data point from the cumulative distribution table. The red and orange lines indicated the mean skid distances selected for the Large and Small aircraft in the DOE-STD-3014. The green line indicates the value of 63.2%, or the mean value of an exponential function. While the cumulative distribution functions are not exactly exponential, they may be approximated as such. The authors of this report postulate that DOE-STD-3014 used this approximation to determine the mean values. Observation of the selected skid distances reveals that for both cases of large and small landings, the DOE-STD-3014 skid distance was approximately 50 ft greater than the value corresponding to the 63.2% exponential mean. While there is no information to confirm this was the case, this report concludes based on the evidence provided, that the landing distances were used along with the 63.2% exponential means. From these, it is postulated that an additional 50 ft in skid distance was added as both a conservative buffer, as well as to address the cases of takeoff. This work will use the postulated logic and the skid distance mean values of 368 ft for large aircraft and 447 ft for small aircraft will be assumed when other information is not available.

Fixed Wing Skid Distance: General Aviation

64. By NTSB definition, a General Aviation aircraft conducting civil aircraft operations are not covered by 14 Code of Federal Regulations Parts 121 or 135 (or 129 for Foreign carriers). Part 121 describes regulations related to major air carriers while Part 125 deals with commuter carriers and "On-Demand" service. Therefore, the general aviation case covers a wide arrange of aircraft. For the purposes of this study, it is assumed that this general aviation category provides a good relative comparison to propeller driven fixed wing UAS.[7] The DOE-STD-3014 defines the mean skid distance of general aviation aircraft as 60 ft; however, there is no supporting

[7]The General Aviation data were collected from NTSB reports that included rotary wing vehicles. Of the 14,034 accident reports documented in the ACRAM study, only 863 or 6% involved helicopter incidents. Given the small number of rotary wing vehicles in the General Aviation skid distance database, the researchers felt the assumption that this category represents fixed wing UAS would still be valid.

documentation other than referencing the ACRAM study. The ACRAM paper generated its database from NTSB data. Some of the initial observations from the data were that in 32.1% of aircraft crashes, there is no measureable skid distance and that approximately 90% of skid distances are less than 135 ft.

65. The ACRAM researchers performed analytical regression analysis on the data. Table 6 shows the results of this analysis.

Table 6: Multiple Regression Analysis for Skid Distance

MULTIPLE REGRESSION ANALYSIS FOR SKID DISTANCE	
Parameter	*Value*
b (intercept term)	0.184
m (aircraft weight-related slope)	0.349
differential intercept coefficients for impact velocity	
0-30 knots: α_1	-0.485
30-60 knots: α_2	-0.310
60-90 knots: α_3	0.000989
90-120 knots: α_4	0.206
> 120 knots: α_5	0.626
differential intercept coefficients for impact angle	
0-10 degrees: β_1	0.471
10-20 degrees: β_2	0.116
20-30 degrees: β_3	-0.236
30-60 degrees: β_4	-0.405
> 60 degrees: β_5	-0.559
coefficient of multiple regression (R)	0.44
sigma	1.32

66. ACRAM researchers provided an example calculation of a 1,500 lb aircraft with impact velocity 60-90 kt and a 20-30 deg impact angle. Based on these three aircraft parameters, data from the chart is combined to determine the relationship to skid distance length, L, as shown below:

$$\ln L = 0.184 + 0.349 \ln 1500 + (-0.485 * 0 - 0.310 * 0 + 0.000989 * 1 + 0.206 * 0 + 0.626 * 0) + (0.471 * 0 + 0.116 * 0 - 0.236 * 1 - 0.405 * 0 - 0.559 * 0)$$
$$= 2.50$$

67. The ACRAM paper uses and recommends a 90th percentile probability to determine skid distance. Using a standard normal distribution and the following equations, the sample calculation has a skid distance of 66.1 ft. This calculation can be seen below:

$$\Pr\{L \leq x\} = \Phi\left[\frac{\ln(x) - 2.50}{1.32}\right]$$

$$x_{0.9} = \exp[2.50 + 1.2816 * 1.32] = 66.1\ ft$$

68. For the purposes of determining LCA, this same approach is used for determining skid distance for the General Aviation category of aircraft (i.e., propeller-driven UAS). The weight will assumed to be the GW of the aircraft, the operating velocity will be assumed as the impact velocity (in the absence of more information), and the glide path angle may be computed from the lift to drag ratio[8] as previously discussed.

Fixed Wing Skid Distance: Commercial Aircraft

69. Incidents involving commercial aircraft are rare events given improved technology and safety processes. The DOE-STD-3014 again cites the ACRAM study; however, the mean skid distance for each paper does not coincide. Like the previous two sections, the DOE-STD-3014 does not give any additional details as to the determination of the mean skid distance selected. The ACRAM document, however, provides the cumulative distribution of Commercial Aircraft skid distances as seen in Table 7.

Table 7: Distribution of Commercial Aircraft Skid Distance

percentile	skid distance
5	160
10	260
15	350
20	440
25	530
30	620
35	710
40	820
45	930
50	1050
55	1190
60	1340
65	1520
70	1730
75	1990
80	2320
85	2760
90	3430
95	4700
mean:	1570

[8]If L/D is unknown, the mean glide path distance can be taken from the DOE-STD-3014.

70. Similarly, to the case for military aircraft, Figure 12 is constructed of the commercial aircraft skid distance cumulative distribution, the mean skid distances provided in the DOE-STD-3014, and the exponential mean line of 63.2%. In addition to these parameters, the mean skid distance as concluded by the ACRAM researchers is provided.

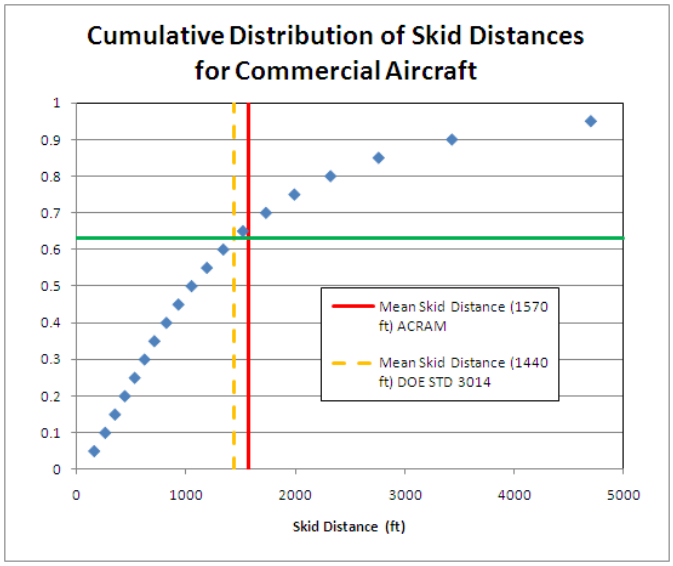

Figure 12: Mean Skid Distance and Probability of Skid for Commercial Aircraft

71. In the case of commercial aircraft, the 63.2% exponential mean line, and the DOE-STD3014 mean distance indication line converge at the same point, 1,440 ft. While this evidence suggests this is how the writers of the DOE-STD-3014 determined the mean value of commercial aircraft skid distance, it is not the same value as provided by the source authors. Because the ACRAM study is the lowest level source of information[9] and the value is slightly higher, a conservative assumption is make to use the larger value of 1,570 ft for commercial skid distances.

72. Initial reaction to the high value of these skid distances was skeptical. A sample of accidents was therefore investigated to determine how valid this mean skid distance could be. Some restrictions placed on the examples were as followed:

- Aircraft must not have crashed in a vertical descent
- Aircraft must not crash on an airfield
- Controlled Flight into Terrain (CFIT) Instances are not considered

73. Table 8 provides some examples of incidents that meet these specified conditions.

[9]ACRAM researchers investigated numerous NTSB reports. Validating each accident analysis was considered a duplication of effort and beyond the scope of this investigation.

Table 8: Mishap Examples for Commercial Aircraft

Comair Flight 5191 Bombardier Canadair Regional Jet CRJ-100ER Attempted Takeoff on Wrong (Shorter) Runway Approximately 900 feet of debris field	Corporate Airlines Flight 5966 BAE-J3201 Impacted Trees Short of Runway Approximately 775 ft of debris path
	
Emery Worldwide Airlines, Flight 17 McDonnell Douglas DC-8-71 Loss of Pitch Control on Takeoff Debris field 1500 x 450 ft wide	NASA/FAA Combined Test Flight Boeing 720 Full-Scale Transport Impact Demonstration 1350 ft Skid from initial ground contact
	

74. Note that the two top instances are smaller business/regional sized aircraft. Conversely, the two lower examples are both four engine transcontinental passenger aircraft. Because commercial operators tend to operate larger aircraft than regional jets, this could have caused the data to be skewed to the higher value. Information regarding these accidents is available in the corresponding NTSB accident reports for Flight 5191, Flight 5966, and Flight 17.

75. A great amount of detail is provided in NASA and FAA technical papers related to the Full-Scale Transport Impact Demonstration. Video of this event shows that the aircraft turns to the left while skidding along the lakebed[10]. While this was the case for this particular event, it is quite likely that incidents could occur that the aircraft does not turn and continues a further distance down the skid path. For the purposes of this effort, these case scenarios appear to support the decision to use the mean skid distance of 1,570 ft for commercial aircraft.

Fixed Wing Combination of Hazard Areas

76. The total skid hazard area can be combined by summing up the lengths of the glide and skid hazard distance. Equation 17 depicts this combination to determine the impact area for Fixed Wing glide. In instances where the impact area due to glide is already determined (i.e., the parametric model for wingspan is used), the impact areas can be combined after the skid distance is multiplied by the hazard width.

[10]Video available online: http://www.youtube.com/watch?v=BNLu-zBkNxw.

$$Hazard\ Area = \left(L_{glide} + L_{skid}\right) \times W_{Haz} \qquad (17)$$

Fixed Wing Kinetic Energy Calculation

77. The Energy for a glide impact may be separated into two stages. This first is the glide descent that can be calculated if the glide airspeed is known using equation 18.

$$KE_{Glide\ FW} = \frac{1}{2} \times \frac{W_{lbs}}{32.2\ ft/s^2} \times \left(1.69 \frac{ft/s}{kts} \times \mathrm{V_{kts}}\right)^2 \qquad (18)$$

78. Since the minimum velocity required to cause a fatality was incorporated into the skid distance in equation 16, the entire skid distance can be considered lethal. For instances where the skid distance cannot be calculated from equation 16, the suggestion is to make the entire skid distance from the above analysis as the lethal skid distance. Note however, if the kinetic energy during glide is calculated as less than lethal, then the skid distance velocity may also be considered less than lethal. This scenario may be the case of a small or micro UAS.

ROTARY WING DIVE

79. As previously seen, the severity of a crash to personnel on the ground is a function of the descent velocity. For rotorcraft, the descent velocity is inversely related to the rotor rotations per minute (RPM) that the vehicle's rotor system is able to sustain. During normal descents, a helicopter's rotor will keep a sufficient RPM to provide enough thrust for a controlled descent rate. Upon closer proximity to the ground, the aircraft performs a flare maneuver, in which the thrust of the rotors decelerates the helicopter to a safe touchdown velocity. A worst case scenario for helicopter flight may be the total and unrecoverable loss of RPM. In this scenario, the blades have decelerated to the point where they are no longer providing any lift. The result is the helicopter descending with nothing but drag to slow it down. This is similar to the aircraft falling with its rotors locked in a non-rotating position. This type of impact can be seen in Figure 13.

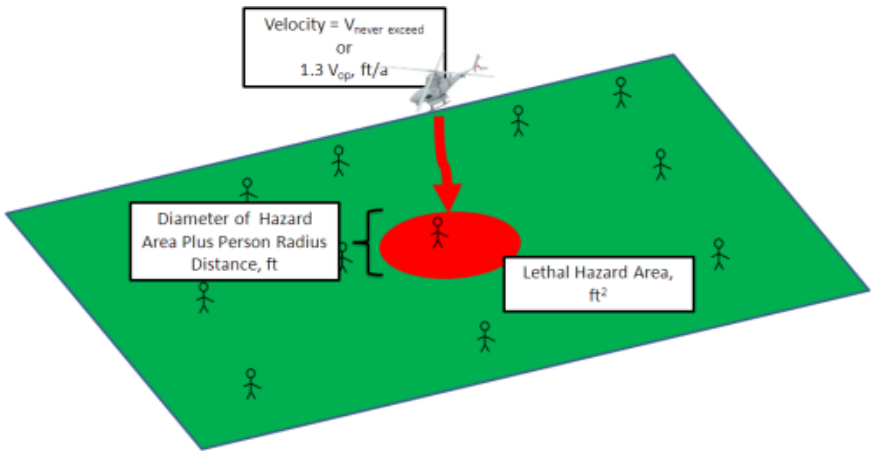

Figure 13: Rotary Wing Vertical Impact (Loss of RPM)

80. Similar to the vertical descent of fixed wing aircraft, the hazard area for a helicopter is dependent on its dimensions. The most obvious choice for a rotorcraft is the rotor blade width itself. The impact area can therefore be calculated as a circle of the radius of the rotors plus the radius of a person. Because most rotary wing aircraft have longer tail sections and they may have non-standard configurations, it is recommended that a 10% buffer be added to the total impact area. The impact area for rotor wing aircraft can be defined by equation 19.

$$IA_{vert\ RW} = 1.10 \times \left[\pi \times \left(R_{Person} + R_{Aircraft}\right)^2\right] \qquad (19)$$

81. The kinetic energy to determine if this impact area is a risk of blunt trauma lethality can be calculated based on the descent velocity using equation 20.

$$\mathrm{KE_{vert\ RW}} = \frac{1}{2} \times \frac{\mathrm{W_{lb}}}{32.2\ \mathrm{ft/s^2}} \times \mathrm{V_{Term}}^2 \qquad (20)$$

82. Here, the descent velocity is assumed to be the terminal velocity of the aircraft. That is, the velocity at which the force of drag acting on the aircraft equals the force of gravity. Determining the force of gravity on an airframe is very simple as it is equal to the aircraft's gross weight. However, measuring the force of drag acting on the airframe is more complicated. To measure the force of drag, the airframe's cross sectional area and drag coefficient must be known. If all of these parameters are known, terminal velocity can be calculated by using equation 21 (reference 1).

$$V_t = \sqrt{\frac{2mg}{\rho A C_d}} \qquad (21)$$

Where:

V_t = Terminal velocity
mg = Mass of aircraft * Gravitational constant = GW of aircraft
ρ = Density of Air
A = Aircraft cross sectional area
C_d = Drag coefficient of the aircraft

83. This report approximates the drag on the fuselage of the helicopter based on published results of fuselage cross section drag coefficients. The coefficient of drag for a blunt body can be difficult to determine without sufficient testing and/or modeling of the airflow field. Lieshman suggests using an approximation of the vertical drag coefficient found for the example fuselage configurations seen in Figure 14 (reference 23).

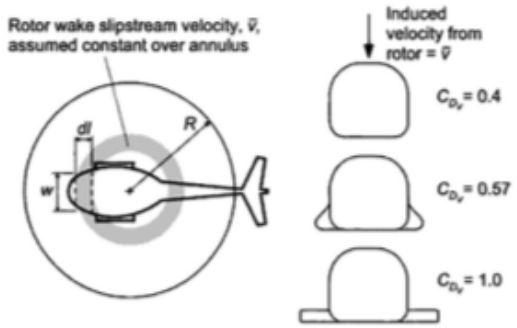

Figure 14: Drag Coefficients of Various Fuselage Configurations

84. Based on the fuselage configuration encountered, the drag coefficient varies. This work assumes a drag coefficient value of 0.5 as an approximation of the type of fuselage configuration typical for military rotor wing aircraft.

ROTARY WING AUTOROTATION RESULTING IN HORIZONTAL-VERTICAL IMPACT

85. In the event that the rotors of the aircraft are still turning sufficiently to provide thrust, a gliding descent is possible. In the event of an engine failure, or another failure requiring the engine to be decoupled from the main rotor (i.e., Tail rotor control loss), the operator may execute a maneuver known as an autorotation to avoid an excessive vertical descent rate. An example of an autorotation impact area can be seen in Figure 15.

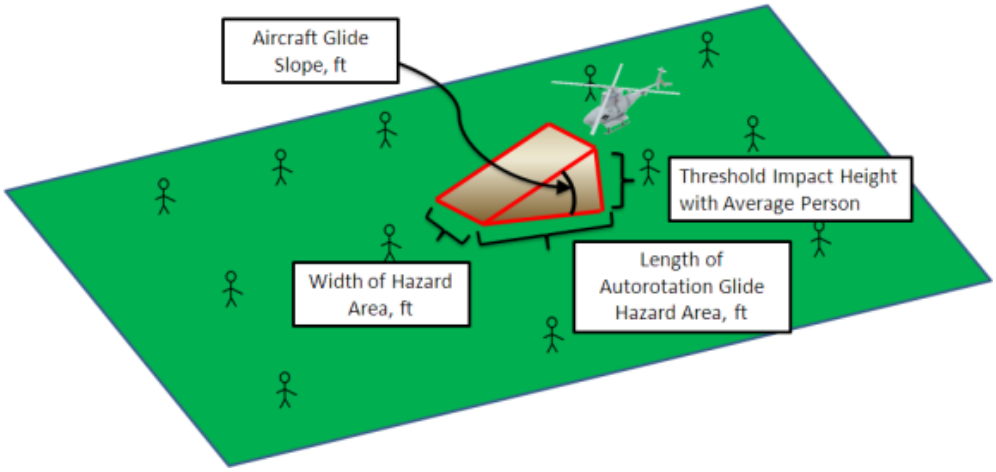

Figure 15: Rotary Wing Autorotation Impact

86. In an autorotation, the aircraft uses potential energy in the form of altitude and kinetic energy in the form of forward velocity to drive the rotor system in the case of a failure mode in which the rotors loose drive power. Once drive power is cut from the rotors, the helicopter descends and uses relative winds to drive the rotor system. The aircraft is giving up altitude (or potential energy) at a controlled rate for kinetic energy to drive the rotor (reference 4).

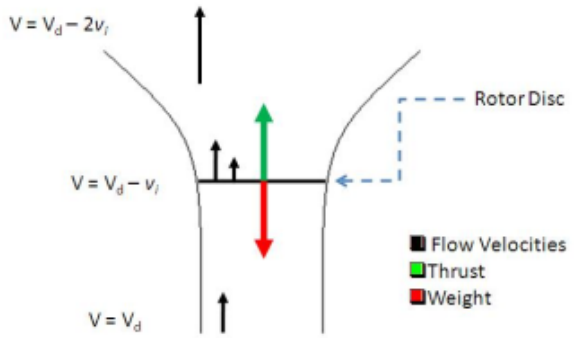

Figure 16: Momentum Theory of Autorotation through a Disc

87. A simple way to model the autorotation for the large variety of sizes and configurations of rotorcraft is with a momentum model. Johnson (reference 20) presents a momentum model. A momentum theory solution states that the following assumptions are made: axial flight (motion only in the vertical), the rotor disk can be modeled as an infinite number of blades and that the disk is strong enough to support pressure differences. As the rotorcraft descends, the relative flow field velocity far below the aircraft is the descent velocity. At the rotor disk, the rotors extract energy from the air, thereby reducing the total velocity by a measureable downward velocity component opposing descent. This downward velocity component is the hover induced velocity. This slows the airstream as it moves past the disk. Downstream of the rotor (which in this case in the up direction), the air separates and results in a relative velocity of the descent velocity minus twice the hover induced velocity. Padfield (reference 31) and Prouty (reference 32) include similar models using momentum theory. Johnson's method was chosen based on the ability to conduct momentum theory analysis on aircraft where not all of the parameters are well known.

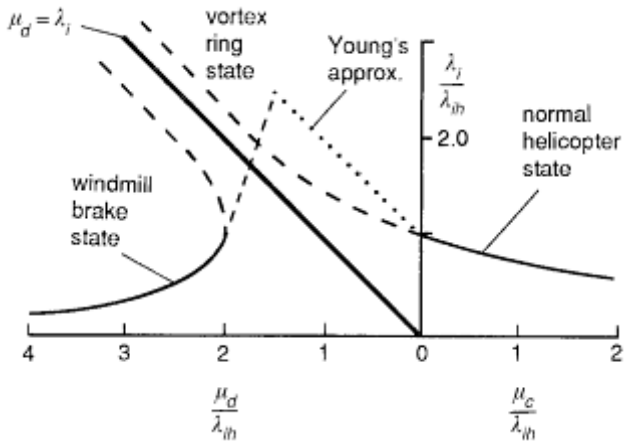

Figure 17: Solutions to Momentum Theory Autorotation and Young's Approximation

88. The physical solutions of this problem are complex and can be seen in Figure 17. Young approximated the ratio of descend velocity to induced hover velocity (reference 23). Johnson built upon this and included an additional term, figure of merit. The result is a straightforward equation found in equation 22.

$$FM = \frac{T\sqrt{T/2\rho A}}{P_{Hover\ Actual}} \qquad (22)$$

Where:
- FM = Figure of Merit
- T = Rotor Thrust
- ρ = Air Density
- $P_{Hover\ Actual}$ = Actual power required to hover
- A = Disk area

89. The figure of merit, as defined by Johnson is the ideal power required to hover over the actual power required. In a steady descent, the thrust can be approximated by the weight of the aircraft and the disk area. If the power required for hover is not known, the value of 0.7 may be used. This is a conservative assumption for the majority of helicopters although more advanced helicopter designs may have a FOM between 0.75 and 0.85 according to Johnson. Analysis shows that the figure of merit is significantly more influential in the value of the ratio of vertical descent velocity to hover induced velocity. Therefore, the model defines $\kappa = 1$, or an ideal rotor efficiency. By estimating the rotor efficiency and figure of merit, it is possible to calculate the decent velocity of the aircraft. By using equations 23 and 24, it is possible to calculate the descent rate.

$$\frac{V_{D\ axial}}{v_i} = -\frac{\frac{1}{FM}-\kappa}{1+3\kappa} - \frac{7\kappa}{1+3\kappa} \qquad (23)$$

Where:
- VD axial = Decent velocity
- Vi = Induced hover velocity
- κ = rotor efficiency
- FM = Figure of merit

$$v_i = \sqrt{\frac{T}{2\rho A}} \qquad (24)$$

Where:
- V_i = Induced hover velocity
- T = Thrust
- A = Disk area
- ρ = Air Density

90. This process can help estimate the descent rate of a helicopter in axial flight conditions. In forward flight, however, the advancing side of the rotor consumes more power in a descent because the relative wind in forward flight gives more energy to the rotor. Leishman shows that estimates of the rate of descent (ROD) in autorotation can be reduced to about half the value required in axial flight. This condition is realized at the airspeed for minimum power under normal flight operations or the maximum endurance speed (reference 23).

91. Another metric can be used to relate the forward velocity to the descent velocity. The assumption here is a linear relationship between forward airspeed and ROD. While reality indicates that this is a non-linear relationship, for the purposes of this effort a linear relationship is acceptable. This relationship can be seen in equation 25.

$$V_{\text{Descent|Forward Velocity}} = V_{\text{D axial}} \times \left(\frac{0.5V_{\text{Forward}}}{V_{\text{Min Power}}}\right) \qquad (25)$$

92. Once the ROD is known, the glide hazard area can be determined. This proposal assumes that an aircraft will autorotate to impact with the ground. That is, there will be no flare maneuver to slow the descent rate of the helicopter. This will give a worst case scenario for impact kinetic energy. As a result, the total hazard area is given by equations 26 through 29.

$$\tan(\gamma) = \frac{V_D}{V_f} \qquad (26)$$

$$L_{\text{Autorotation}} = \frac{H_{95\text{th}}}{\tan(\gamma)} \qquad (27)$$

$$W_{\text{Haz}} = 1.10D_{\text{Main Rotor}} + (2R_{\text{Person}}) \qquad (28)$$

$$IA_{\text{Auto RW}} = (W_{\text{Haz}}) \times (L_{\text{Autorotation}}) \qquad (29)$$

Where:

γ = Decent angle
V_d = ROD
V_f = Forward Velocity
$L_{Autorotation}$ = Length of autorotation hazard area
H_{avg} = Height of 95th percentile male
W_{haz} = Width of hazard area
R_{person} = radius of 95th percentile male
$D_{main\ rotor}$ = Diameter of main rotor
$IA_{auto\ rw}$ = Hazard area for rotor wing autorotation

93. Finally, the Kinetic Energy for the autorotation can be calculated using the magnitude of the descent and forward velocities as defined in equation 30.

$$KE_{\text{Auto RW}} = \frac{1}{2} \times \frac{W_{\text{lb}}}{32.2\ \text{ft/s}^2} \times \left(\sqrt{V_D^2 + V_f^2}\right)^2 \qquad (30)$$

94. It should be noted that there was a lack of skid distance in the rotorcraft model glide description in Figure 8. Information from the DOE standard suggested a skid distance of 0 for helicopter crashes. This value seems to make logical sense when considered that rotor aircraft in the DOE paper suggests an average crash angle of 60 deg. Videos of helicopter crashes appear to confirm the assumption of a 60 deg impact angle, but not the zero skid distance assumption. Therefore, an investigation was done to evaluate this skid distance for common helicopters.

Helicopter Skid Distance Investigation

95. NTSB reports are categorized by several attributes but the most relevant to this study are "type" of report and "aircraft damage". The type of investigation would involve either an incident report or an accident report. Incident reports contain very little information and research proved it was quite difficult to determine any metrics from this data. Accident reports have more data and involve some type of failure whether it is mechanical or human related. For the purposes of investigating rotary wing UAS, it was assumed that accident data would be more useful. The aircraft damage was separated into Minor, Substantial, and Destroyed. Minor damage means the aircraft is still flyable, substantial means repairs must be made prior to resuming flight, and destroyed indicates the aircraft had to be salvaged. Minor and substantial damage related reports typically lacked details and resulted in small area related data. For the purpose of data collection, it was assumed that the destroyed data would provide the most useful information and would be more appropriate to model rotorcraft UAS crashes.

96. Fifty-two NTSB reports were reviewed for information regarding both skid distance and debris fields for helicopters. The average skid distance for the cases examined was 77 ft with an average potential debris area of 8,800 ft^2. Further examination of the data, however, reveals that these values are inappropriate for most helicopter related incidents. One accident analysis skews the skid distance average higher than it possibly should be.

97. NTSB report SEA06GA158 describes a helicopter that crashed because of CFIT. While there were no witnesses, the pilot in control was known for acrobatic low level flight. Additionally the investigation teams found no mechanical failures leading to the incident. The result was a high velocity, high energy impact that resulted in a total distance travelled of 1,200 ft. The mishap also occurred in a mountainous area where the terrain may have added to the considerable length of this event.

98. Removing this one particular event, results in a skid distance average of 55 ft. This value may also be too high for most helicopter accidents. Removing the next five largest skid distance crashes, or the top 10%, resulted in a mean skid distance of 24 ft. Out of the 52 events looked at for the purposes of this evaluation, 27 had skid distances of 0 ft. These zero skid distant events included autorotation, wire strikes, loss of control, tail rotor impact, mid-air collision, and CFIT into water. This suggests that in most of the possible failure modes of helicopter crashes examined, there exists some possibility of 0 ft skid distance.

99. Given this information, there was an attempt made to decompose the problem based on the types of helicopter failures. Figure 18 plots the average skid distance of a group of failure mode categories along with the percentage of those failure modes.

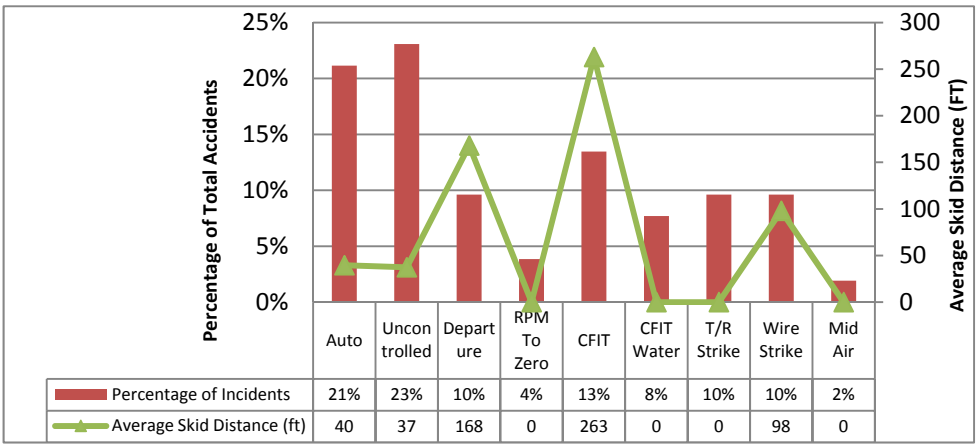

Figure 18: Skid Distance with Respect to Failure Mode

100. From Figure 18, autorotation and uncontrolled failure modes have mean skid distances of 40 and 37 ft, respectively. These failure mode categories represent 44% of the total number of accidents. The cases of RPM to zero, controlled flight into water, tail rotor strike, and mid-air collision all have mean skid distances of 0 ft representing 24% of the total incidents. It should be noted that the data collected for these events represent the consequence of failure events and that the causes of these events are very different. The instances of CFIT, departures, and to a lesser extent Wire Strike resulted in larger mean skid distances. The final three categories represent 33% of the incidents investigated.

101. The cases of CFIT, controlled fligth into water, and mid-air collision are all the result of human lapses in navigation and/or traffic control. It will be assumed that either due to advanced avionics or operational guidance, these aforementioned cases may be ignored for the purpose of developing a UAS crash lethality model. The RPM to Zero may be included with the autorotation data, since an autorotation was probably the correct action to take in these accident instances, but the success was not complete. The case of departure will be included with uncontrolled flight since for all intents and purposes, the loss of the main rotor represents the ultimate loss of rotorcraft control.

102. Making these simplifications reduces the total number of reports to 40 cases. The mean skid distance thus becomes 55 ft. A total of 22 of these incident reports had a skid distance of 0 ft representing a little over half. Distribuiting the results into the remaining failure modes of Autorotation, Uncontrolled Flight, Tail Rotor Strike, and Wire Strike results in Figure 19.

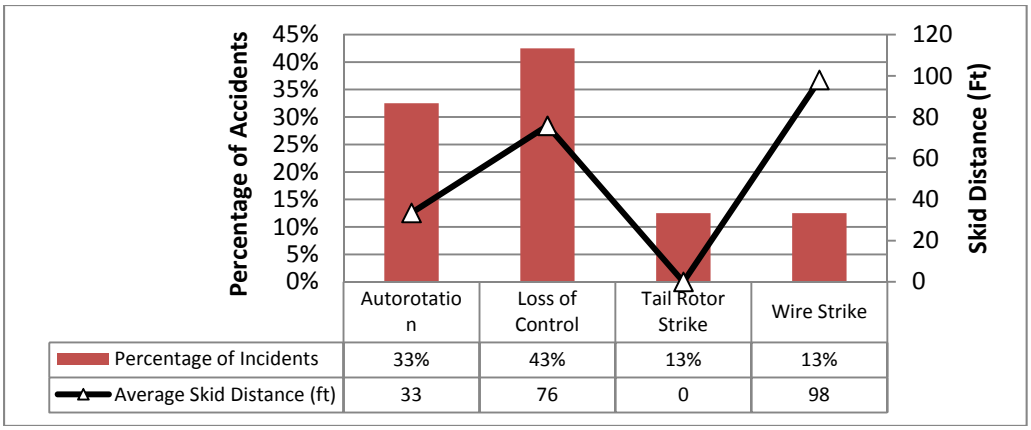

Figure 19: Skid Distance for Helicopter Failure Modes

103. The autorotation represents 33% of the incidents and had a mean skid distance of 33 ft. Loss of Controlled Flight accounts for 43% with a skid distance more than twice that of autorotative flight at 76 ft. The remaining cases involve tail rotor strikes and wire strikes. The tail rotor strike has a mean skid distance of 0 while Wire Strikes have the highest mean skid distance of these categories at 98 ft.

104. Wire strikes occur due to aircraft inadvertently flying into wires or cables that have been placed along the pilot's intended flight plan. There are two mitigation strategies that can be used to avoid wire strikes. The first is flight planning, where the intended operator will create a planned path for the aircraft to fly that will avoid known transmission wires and other obstacles along the intended route. Terrain flight planning has been demonstraighted by Japan with unmanned rotor aircraft servicing rural high powered electric lines. This was done by including transmission lines in the flight planning software where an operator can visualize the transmission towers and cables. The work is a push to develop rotorcraft UAS that can autonomously inspect high voltage high energy transmission lines for damage (references 17 and 37). The second method of mitigation is to see the wires and avoid them in-flight. Wires in flight are very difficult to see even for experienced aircrew. Some efforts have been made to include bright markers for pilots to identify the transmission wire hazards. Obstacle detection using various methods have been used to give pilots greater time to react to wirestrikes (references 3, 7, 35, and 36). These systems were initially heavy and expensive, but have now miniaturized to be included in unmanned vehicles.

105. The optimal solution is to use both flight planning and in flight obstacle avoidance. The combination of the two has been investigated by Eurocopter (reference 13 and 36) a. While this technology currently requires a "man in the loop, it is not unreasonable to believe that the combination of proper flight planning with detailed route databases and new advances in wire detection technology will make future wire strike accidents exteremely rare events. Therefore, wire strikes for unmanned rotorcraft will not be considered as part of this effort's data source as is left for future research to determine the impact of obstacle avoidance systems to crash lethality.

106. When a tail rotor strikes an obstacle or object in a conventional helicopter, the result is the loss of antitorque compensation. Normally, the tail rotor generates a torque around the aircraft's center of gravity (CG) to counteract the torque being driven to the main rotors by the power plant(s). When the tail rotor impacts an obstacle, it typically fails resulting in the loss of this counteracting torque. The aircraft then will begin to spin violently in the direction opposite of the main rotor rotation unless the engine is disengaged from the main rotor. If a tail rotor strike were to occur, a pilot should arrest power and lower collective input to enter autorotation. However, if this is not done in time, the aircraft will enter a spin opposite the direction of the rotation of the rotor system which quickly increases in speed. This state will lead to uncontrollable flight and subsequent loss of the aircraft. As a result, it was determined that tail rotor strikes be combined with loss of control of the aircraft.

107. The result of removing the wire strike incidents and combining tail rotor strikes with loss of control events results in a refined finding that can be seen in Figure 20. The loss of control event appears to average twice the skid distance of autorotations. Examination of the remaining incidents reveals, however, that one event had a 500 ft debris path which is substantially higher than the next largest skid distance and skews the mean distance for this category.

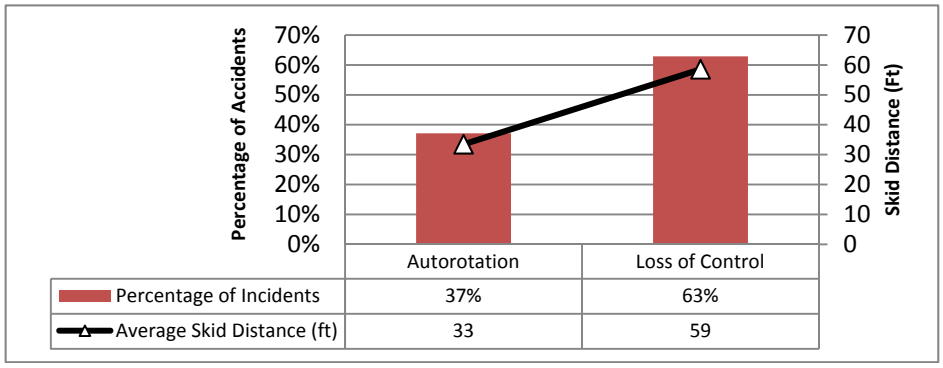

Figure 20: Skid Distance for Helicopter Failure Modes

108. NTSB report LAX06FA156 describes a Robinson R44 II helicopter flight that crashed on 1 May 2008. Subsequent investigation found a primary debris path extended 500 ft east of the main wreckage site. An additional debris path of papers and light cockpit materials extended beyond the 500 ft debris path 400 ft to a total distance of 900 ft away from the main wreckage site. Examination of the rotor system linkages and fuselage suggest that the main rotors impacted the fuselage while in flight. Investigators' conclusion was the helicopter crashed from loss of control and the divergence of the main rotor blade system from its normal rotational path for undetermined reasons.

109. Closer investigation into the report revealed that the main rotor separated and, according to accident investigators, probably cut through the fuselage. Therefore, items found within the debris path that in most accidents would indicate an initial impact with the ground (i.e., The right side pilot's door, large chunks of fiberglass and plexiglass) may have come off of the aircraft in

flight before impact. It may be impossible to judge the exact skid distance for this event. Rather than make some assumptions as to the nature of this event, the event is discarded. The results of this task are presented in Figure 21.

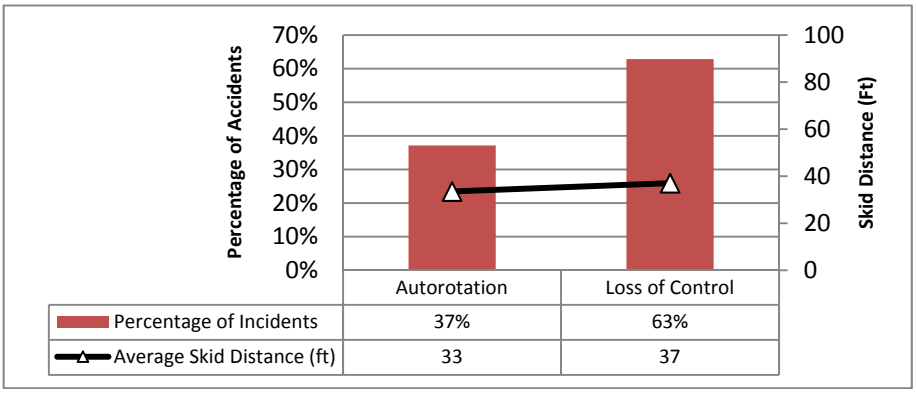

Figure 21: Skid Distance for Helicopter Failure Modes

110. Figure 21 suggests that the skid distance for helicopter aircraft are relatively close whether during an autorotation or loss of control event. To simplify the results into a single number, the events are averaged to 35 ft.

111. A complete investigation into the hazard area of helicopters would not be complete without addressing the topics of blade debris and fragmentation. Video evidence confirms that incidents involving helicopter impacts with the ground often result in fragmentation to disintegration of the main rotor blades along with a considerable amount of debris. Two methods for attempting to evaluate the risk to personnel were examined. The first is a historical approach using NTSB data to create a parametric model of typical debris area. The second involves building a model related to main rotor blade failure or fragmentation.

HELICOPTER BLADE THROW AND FRAGMENTATION

Blade Throw Model

112. The blade throw model presented here represents the collection of effort from literature searches, video observations, modeling, and analysis. The main rotors of a helicopter have a large amount of energy stored while operating; making the rotors particularly dangerous to personnel should a failure occur. This section describes some of the historical models that were considered, some of the theory and assumptions used to simplify the problem, and a final model product that while conservative should provide real world relevant data for driving the analysis of determining the casualty expectation number.

113. Research was done to identify any previous literature on the topic of helicopter blade/fragmentation throw. As of this writing, the researchers are unaware of any published findings concerning this general topic. There are formal documented reports on rotor blade separation from the main rotor mast; however, these are all limited to high inertia teetering rotor mast helicopters such as the UH-1 Huey and more recently the Robinson R22 and R44 family of helicopters. Due to configuration differences, the teetering masthead configuration in this data would likely be ineffective at modeling non-teetering mast configurations. Varying rotor head designs can be seen in Figure 22.

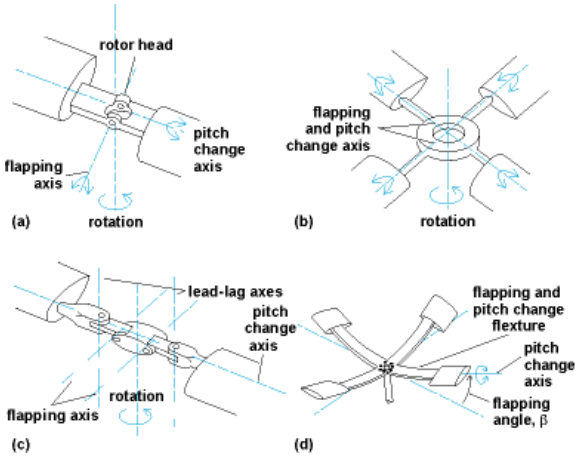

Figure 22: Principal Types of Rotor Hubs

(a) Teetering (semi-rigid) rotor head. (b) Gimbaled rigid rotor. (c) Fully articulated rotor head. (d) Hingeless rotor.

114. While no documentation could be found in regards to the risk of a helicopter rotor, there has been significantly more interest in the risk analysis of wind turbines within the past 30 years. Due to the gaining prevalence and use of wind turbines as a source of renewable energy, there has been an increase of concern regarding the safety of these units and the perceived risk to the public. This is even more important as new wind farms are being installed in ever closer proximity to residential areas.

115. The most thorough approach to wind turbine blade risk was done by Macqueen et al in Risks Associated with Wind-Turbine Blade Failures (reference 25). The authors describe the basic equations of motion of the failed blade, the initial conditions of a runaway blade, the characteristic of the blade known as tumbling, blade throw calculations with tumbling, additional discussion on the effects of lift, and finally proposes a more thorough three-dimensional model with rigid body dynamics for higher fidelity results. More recently, Morgan and Bossanyi wrote about the risks associated with ice shedding from wind turbine blades (reference 28). While not exactly the same as a blade being thrown, the dynamics of an ice fragment shedding from a blade is very similar to that of a main rotor blade itself. Morgan and Bossanyi recognized the conclusions that Macqueen et al made present a somewhat simpler model for investigating the maximum safety threshold for ice fragments. The model presented in this report will draw

references from both papers to develop a model that is robust enough to give accurate results for helicopter rotor blades while simple enough to allow relatively quick feedback to an investigator.

Ballistic Trajectory Model

116. The simplest method for modeling blade and fragment debris throw is using a ballistic trajectory with no air resistance. This type of model assumes that the effects of drag due to air resistance are negligible compared to that of gravity. This is the case presented in Figure 23 for a blade or fragment separating from the aircraft with close proximity to the ground.

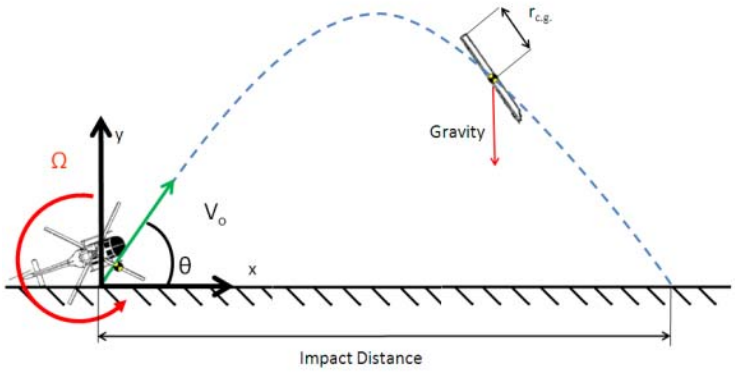

Figure 23: Ballistic Trajectory of Rotor Blade with no Wind Resistance

117. The equation to determine the horizontal range of the projectile when ignoring air resistance can be simply computed by equation 31.[11]

$$X = \frac{V_o^2}{g} \sin 2\theta \qquad (31)$$

Where:
X = Horizontal distance traveled
V_0 = Initial velocity of rotor blade
g = Gravitational constant
θ = Release angle between velocity vector and horizon

118. Note that for a complete blade failure, the radial CG, or r_{cg}, is half the rotor radius. For a fragment of the blade tip being shed, this would be the radius of the blade, thereby resulting in a much higher initial condition. The maximum distance the projectile can achieve downrange in the absence of air resistance is reached when the release angle is 45 deg. This reduces the equation to:

[11]For a complete derivation of the range for a projectile while neglecting air resistance, please see McGill and King's Introduction to Dynamics or any other introductory level dynamics textbook. In addition to the assumption of negligible air resistance, the derivation assumes the path is sufficiently limited that the gravitational constant of the Earth is a constant.

$$X_{max} = \frac{V_o^2}{g} \qquad (32)$$

119. This equation suggests that as a worst case scenario, the maximum blade distance achieved could be determined based solely on the initial velocity. Macqueen et al suggest that the addition of air resistance will have three significant impacts to the range calculated by equation 32.

Tumbling Drag Model

120. This section describes the effects to trajectory and distance throw as the result of adding air resistance. It first describes some of the initial affects of adding air resistance. It then gives a description of a common airfoil similar to the cross section of a rotor blade or fragment. After introducing the airfoil, this section makes the case that an airfoil will tend to tumble through the air rather than maintain one specific orientation. Finally, this section describes the previous efforts to describe blade and fragment throw distances with air resistance considered.

Adding Air Resistance

121. The first major impact is a limitation known as the sonic limit. As blade tips reach supersonic speeds, their efficiency decreases exponentially while, the drag encountered climbs exponentially. At sea level, the speed of sound is approximately 340 m/sec, which if this value is plugged into equation 33, limits the maximum blade throw distance to just under 12 km or just under 7.5 miles. This is the limit for any type of fragment or blade being launched from the ground for both helicopter rotors and wind turbines regardless of mass, shape, or rotor dimensions.

122. The second major impact on an objects trajectory is drag on the projectile. The drag force opposes motion through the air opposite to the direction of motion. It is proportional to the square of the velocity and therefore plays an important role particularly over longer distances and high speeds. The effects of drag will be discussed further in the Tumbling Drag model.

123. Finally, the third major impact on air resistance is the effects of wind. For wind turbines, wind is the resource being consumed and a very likely culprit for blade failure should certain thresholds be exceeded. Therefore, in the work done by Macqueen et al for blade fragmentation, as well as Morgan and Bossanyi's work for ice shedding, it is assumed that the prevailing wind may carry the blade or fragment through the air. While the previous two impacts limit trajectory, this one in particular may increase the total range.

Airfoil Description

124. To understand the effects of wind on a rotor, it is important to understand some fundamental aspects of airfoil design. A simplified cross-section of a rotor blade will show a typical airfoil design. A loaded standard airfoil can be seen in Figure 24.

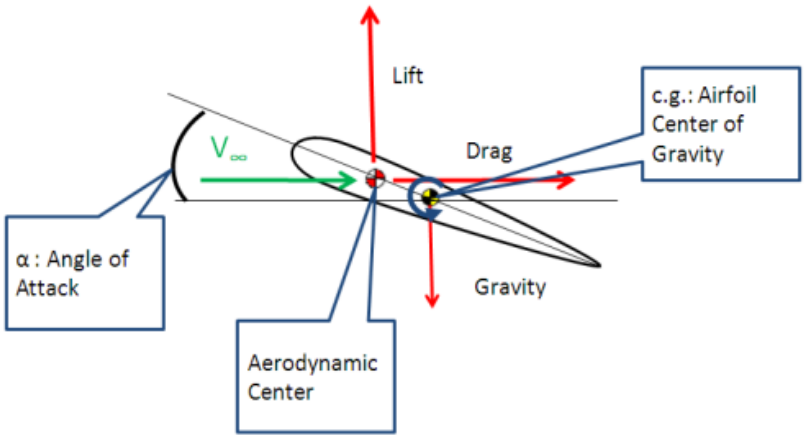

Figure 24: Standard Loaded Airfoil

125. The forces, shown in red, reflect the aerodynamic and gravitational forces exerted on the airfoil section; they are lift, drag, and gravity. The aerodynamic forces act around the airfoil's aerodynamic center, which is typically placed at the airfoils quarter chord. The blue arrow indicates a moment about the CG that would counter the moment generated by the forces on a normal blade. Figure 25 shows how this moment can vary depending on the orientation of the airfoil.

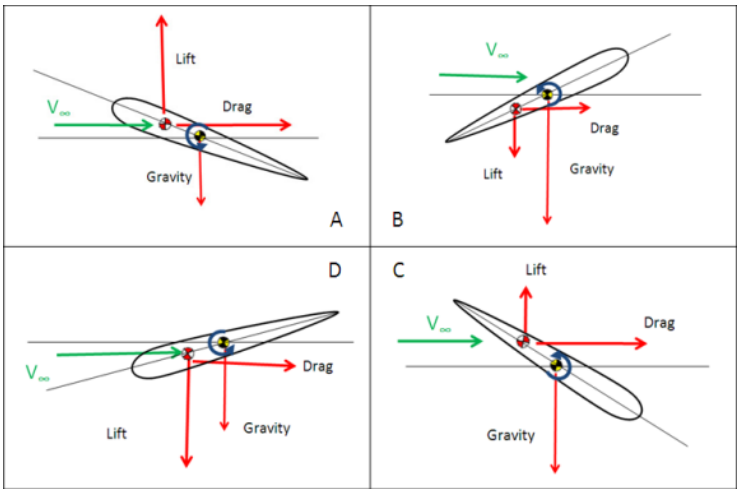

Figure 25: Airfoil at Varying Orientation

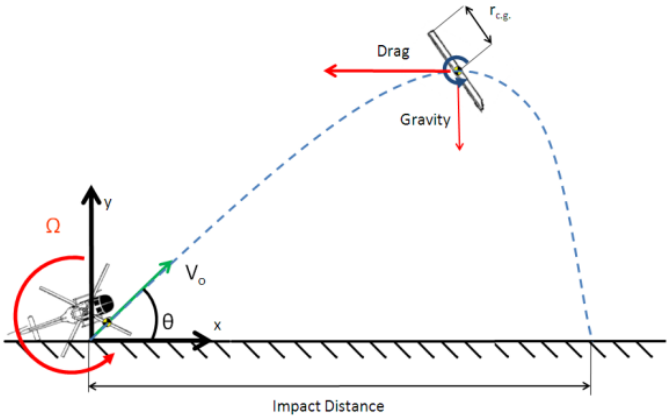

Figure 26: Blade Trajectory for Tumbling Blade

126. Figure 26 shows why an aerodynamic shape such as a helicopter rotor blade, wind turbine blade, or aircraft propeller would, tumble after being thrown through the air. Assuming that the airfoil cross section is initially in a positive angle of attack (AOA) the lift and drag forces result in a moment about the CG. This results in a rotation about the CG, further increasing the AOA. The lift force will first increase with increasing AOA and then decrease substantially after reaching a maximum while the drag component will continue to increase until the section has become perpendicular to the direction of motion. Throughout this process, the forces are producing a moment about the CG results in the object wanting to rotate to a higher angle. When this happens, the lift decreases while drag increases until the airfoil section is perpendicular to the velocity. Drag, still acting on the aerodynamic center, continues to force the roll. Eventually the cross section is headed into the wind in a "tail first configuration" (B). With a moment continuing to act on the airfoil proportional to the forces involved, the aerodynamic center shifts and the result is a lift and drag force that creates a moment opposite of the rotating motion. Due to the shape of the airfoil cross section in the tail first configuration, the lift performance will be considerably less than that of the standard orientation. Therefore, the opposing moment will be less. Additionally, the forces are dependent on the velocity squared term. The drag encountered during the first stage (A) will decelerate the section such that even if the efficiency of the airfoil were the same from both ends, the forces would be reduced due to the reduction in velocity. The net result is angular motion and inertia about the CG. The orientation in (C) will tend to further increase the current motion, while (D) will attempt to oppose the motion. Note that, the airfoil could also move in the opposite direction with similar results. This assessment assumes that the velocity is changing due to wind resistance. Should the velocity be kept at or near constant, it is feasible, however as Macqueen points out very unlikely, that the blade will achieve a sort of equilibrium state. If this were to occur, it would be more likely in the tail first orientation.

127. Since the case of tumbling is the most likely scenario and neglecting air drag could be considered overly conservative, a means of modeling the tumbling blade or fragment must be created. To do so, a return to the airfoil is required. From the example of Figure 24, one anticipates the blade or fragment to rotate while in flight. As long as the period of rotations is

sufficiently fast when compared to the total flight, the average lift vector will essentially be zero. With lift eliminated, the following set of equations can be derived from the free body diagram.

$$m\ddot{x} = -\frac{1}{2}\rho A C_D V(\dot{x} - W) \qquad (33)$$

$$m\ddot{y} = -mg - \frac{1}{2}\rho A C_D V\dot{y} \qquad (34)$$

$$V = \sqrt{\dot{x}^2 + \dot{y}^2} \qquad (35)$$

128. For the purposes of building a blade throw model for helicopters, some assumptions are made in order to pull from the best of both of these model results. In order to determine the largest LCA, it will be assumed that the wind is in the same direction of the blade throw. This reduces the degrees of freedom from 3 to 2. Distance will be measured from the rotor hub and wind speeds will assumed to be sustained (i.e., no accounting for gusts). The tool will provide the ability to evaluate both the effects of an entire blade and a fragment.[12]

The Lift Case

129. A third and final case could be considered where the blade or fragment moves through the air in such a way that an equilibrium condition exists that can result in a net lift occurring on the blade. A net lift will result in the airfoil effectively gliding away drastically extending the range. Macqueen et al investigated this possibility as a worst case scenario in which the "fragment orientation continuously (and maliciously) adjusts itself to maintain the upwards component of the lift force." Unlike the case tumbling case, the researchers could not replicate this effort. Due to the extremely low probability of this occurring, it will not be evaluated for the purpose of this study. The lift case can be seen in Figure 27.

[12]An entire blade may have a lower drag parameter than a tip fragment. This can equate to considerable distances from the blade meeting and in some cases exceeding the maximum distance for a tip fragment. This is especially true in very high velocity wind.

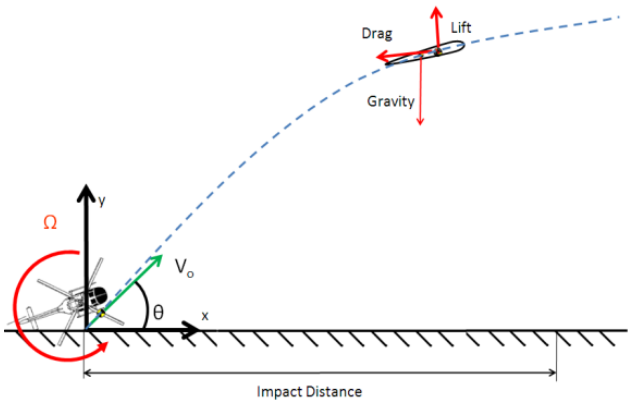

Figure 27: Blade Trajectory for Lift Case

Model Selection

130. The following summarizes the processes and equations used by this effort to model the effects of a rotor blade or fragment becoming dislodged from an air vehicle upon impact with the ground. The equations of motion are provided below:

$$m\ddot{x} = -\frac{1}{2}\rho A C_D V(\dot{x} - W) \qquad (36)$$

$$m\ddot{y} = -mg - \frac{1}{2}\rho A C_D V\dot{y} \qquad (37)$$

$$V = \sqrt{\dot{x}^2 + \dot{y}^2} \qquad (38)$$

Using Newtonian approximation methods and assuming changes are small these equations are reduced to:

$$\dot{x}_f = \dot{x}_o + \Delta\dot{x} = \dot{x}_o + \ddot{x}\Delta t \qquad (39)$$

$$\dot{x}_f = \dot{x}_o + -\frac{1}{2}\frac{\rho}{m} A C_D V(\dot{x} - W)\Delta t \qquad (40)$$

$$x_f = x_f + \left(\frac{\dot{x}_f - \dot{x}_o}{2}\right)\Delta t \qquad (41)$$

$$\dot{y}_f = \dot{y}_o + \Delta\dot{y} = \dot{y}_o + \ddot{y}\Delta t \qquad (42)$$

$$\dot{y}_f = \dot{y}_o + \left(-g - \frac{1}{2}\frac{\rho}{m} A C_D V\dot{y}\right)\Delta t \qquad (43)$$

$$y_f = y_f + \left(\frac{\dot{y}_f - \dot{y}_o}{2}\right)\Delta t \qquad (44)$$

131. By selecting a timeframe small enough to ensure the small changes assumption is valid, the change in velocity at each time increment can be determined. The positions are then numerically summed to represent the position of the blade or fragment.

132. Given appropriate input parameters, the algorithms described above should output total downrange distance of the rotor blade. Because of the tumbling assumptions, drag will cause the artifact to slow down and reduce its kinetic energy. Therefore, the kinetic energy is calculated at each instance. Only the distances associated with kinetic energies below the lethal threshold as specified in section will be considered in the maximum range.[13]

Helicopter Fragmentation Area

133. An analysis was done to investigate an appropriate debris area size for a typical helicopter crash. This discussion is available in the following paragraphs. In order to keep results consistent with the skid distance results, the same events used in the reduced data were used for the debris area instance. The results can be found in Figures 28 and 29.

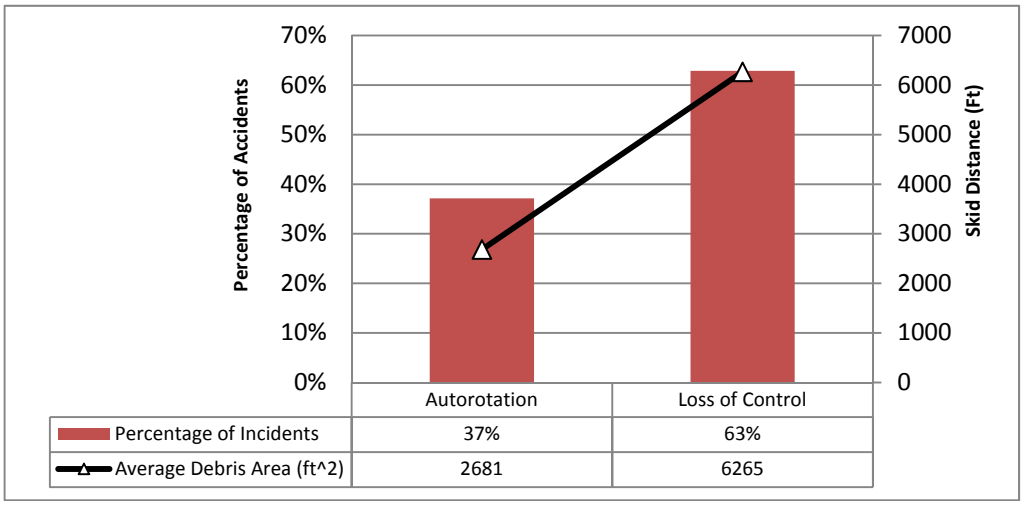

Figure 28: Helicopter Failure Modes Debris Area

[13]Note that the vertical velocity component of the fragment will be minimal at the height maximum. As a result, it is possible to have a non-lethal kinetic energy in the middle of the blade of fragment trajectory. For the purposes of this effort, however, these cases are excluded, as the resulting gravitational force acting on the fragment as it descends will speed the piece back up to a lethal level.

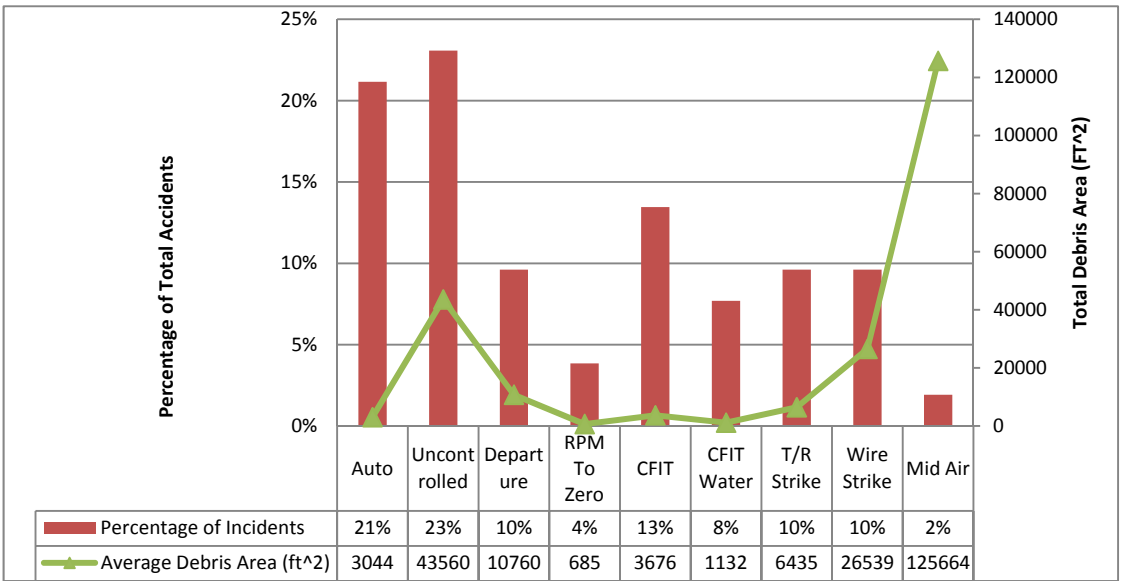

Figure 29: Helicopter Failure Modes Debris Area

134. Using a weighted average, the average debris area for a typical helicopter crash can be approximated as 4,900 ft^2. However, it should be noted that there were inconsistencies with the NTSB reports used to assimilate this data. Some accidents would contain wreckage information including a description of the debris field while others would not. Still others would describe that all parts were found "at the scene". Pictures and television coverage confirmed that in many of these cases, the "debris field" is quite small and is contained within the size of the helicopter. For instances where debris was present and a measureable distance away from the helicopter, a circle of radius equal to the distance between the final crash site and debris component was used. In cases where this information was not present or where descriptions/pictures suggest a small debris area, it was assumed that the debris area could be represented by the disk area of the main rotor. This required researching the dimensions of the helicopters involved in the crash events.

135. For the vast majority of helicopter crashes, the debris field was within an order of magnitude of the size of the helicopter. The cases where this was not the case was most often where mechanical failures or pilot error resulted in catastrophic loss of main rotors at speed and at altitude spreading debris over a large area.

136. NTSB Aircraft Accident Report AAR-09/02 describes the mid-air collision examined in this effort. The two aircraft were both Phoenix, AZ, television news helicopters and were both covering a high speed pursuit. After the collision, both helicopter fuselages nosed down and impacted the ground at high vertical speed resulting in zero skid distance. The debris caused by two helicopter main rotors impacting each other at altitude over a populated area resulted in a significantly wider debris area. Reporting of the debris may also have been substantially higher given the urban environment.

137. From the preceeding work, the researchers have defined the mean skid distance and debris area for civilian helicopter operations. The goal of this study, however, is to develop a crash lethatlity model that will include the likelihood of lethality based on aircraft parameters. Therefore, one must be able to scale data results from the limited data from large cargo carrying platforms to micro and miniature UAS.

138. Determining a parametric model relationship between aircraft characteristics and historical crash details of both skid distance and debris area were more difficult than the determination of general skid distance. A simple scatter plot of the data shows a large degree of variance in terms of skid distance and debris area. In order to parameterize these relationships, the original 52 incident dataset was used to provide the statistical data. Then, the results of skid distance and debris area were compared to multiple different aircraft related parameters to determing their correlation. Rotor diameter, GW, Velocity Never Exceed (Vne), and the translational kinetic energy of the aircraft were all parameters used in trying to build a viable model. The final parametric model was used by drawing experience of the calulcation for blunt trauma lethality. The logarythmic relationship was established first between the debris area and the energy term. The equation for this relationship is shown below.

$$LN(Area) = 0.339 * LN\left(KE_{ft-lb}\right) + 1.575 \qquad (45)$$

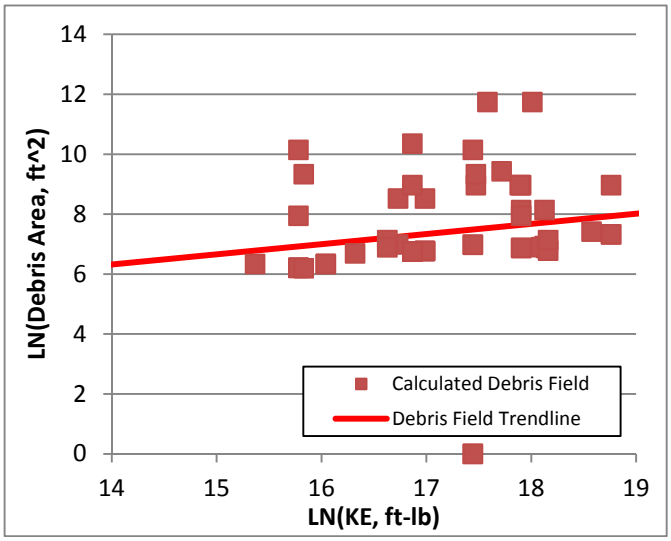

Figure 30: Debris Field Statistical Data

139. The resulting R-square term for this relationship was only 0.02973 with the broad data range. Reducing the data set rather to that used for the average distances resulted in a better fit. The R-square value roughly doubled. While still low, the 95% confidence interval encompases most of the data points remaining in the reduced data set as shown.

140. Given the limited data set, it was felt that this is the best parametric model available.

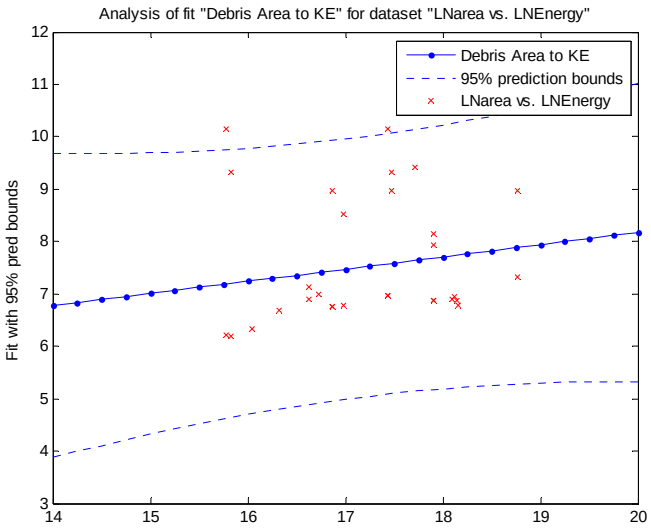

Figure 31: Parametric Model for Rotor Wing Debris Area

141. For skid distance, the same process was used to try to identify a similar relationship. The result was an equation similar to the debris area and provided below.

$$LN(Skid\ Distance) = 0.2817 * LN\left(KE_{ft-lb}\right) + 2.854 \qquad (46)$$

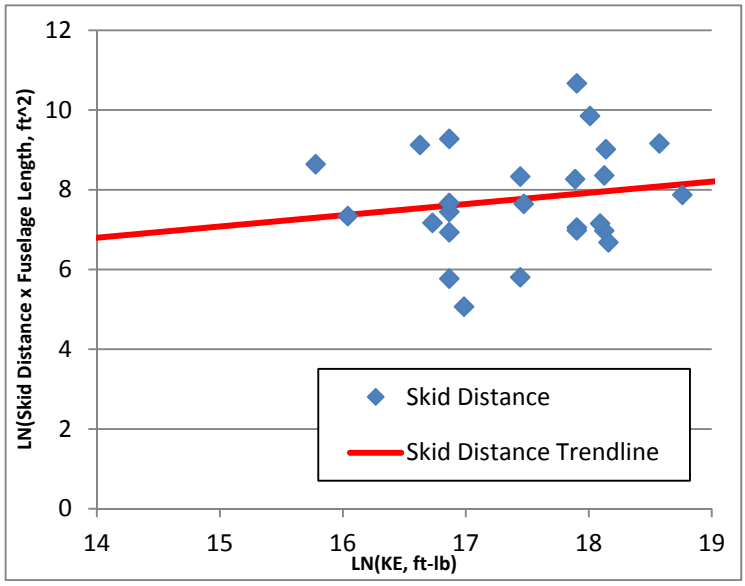

Figure 32: Skid Distance Statistical Data

142. Originally, the skid distance alone was used to attempt to correlate the data. The additional of the aircraft length greatly increased the performance of the model to the data set. This suggests that the length of the aircraft is an important factor in the size of the skid distance of a helicopter. From a practical standpoint, this makes sense as a larger and longer helicopter will cover a greater amount of area when it impacts the ground over a smaller shorter aircraft. The results of this curve fit with 95% confidence intervals are shown in Figure 33.

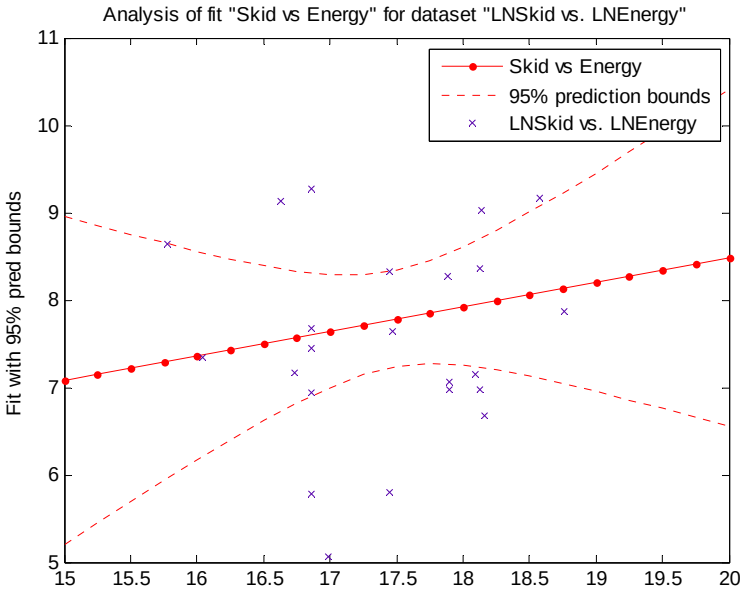

Figure 33: Skid Distance Parametric Model

143. The parametric models for Rotary Wing Debris and Skid Distance models developed were not found to be sufficient accuracy for inclusion into LCA. Further research is required to provide additional data to improve the accuracy of the regression plots. They have been provided here as guidance from which further effort can be applied.

SHELTER FACTOR REDUCTION FOR KINETIC ENERGY

SHELTER ABSORPTION CALCULATION

144. The lethal area discussed above applies to personnel who have no shelter to protect them. Shelter can reduce the likelihood of a fatality by absorbing the kinetic energy of the crashing aircraft. As a shelter deforms, breaks, and moves because of an aircraft impact, it is absorbing energy from the crash. The final or net kinetic energy because of a vehicle crash can therefore be calculated using equation 47. If the net kinetic energy is negative, then it must be assumed that the structure absorbed the impact of the UAS and prevented any penetration.

$$\mathrm{KE}_{\mathrm{net}} = \mathrm{KE}_{\mathrm{Aircraft|Blunt}} - \mathrm{KE}_{\mathrm{absorbed}} \qquad (47)$$

145. Note the differences in structure performance between roof-top and sidewall. For vertical impact flight termination, it is recommended to use the roof type kinetic energy absorption values. For gliding and autorotative flight, the sidewall absorption should be used. The values for roof and sidewall are provided in Tables 9 and 10, respectively (reference 14).

Table 9: Roof Kinetic Energy Absorption Values

Roof Type	% Invulnerable Area (nominal), LA_roof	KE absorbed by roof (ft-lb) ΔKE_n
4 in. Reinforced Concrete	10	10000
14 in. Reinforced Concrete	15	200000
Plywood/Wood Joist (2x10 at 16 in.)	5	50
Gypsum/Fiberboard/Steel Joist	5	25
Plywood Panelized (2x6 at 24 in.)	5	50
2 in. Lightwiehgt Concrete/Steel Deck and Joists	7.5	2000
Medium Steel Panel (18 gauge)	7.5	1500
Light Steel Panel (22 gauge)	7.5	1000
Steel (automobile)	2.5	200

Table 10: Side Wall Kinetic Energy Absorption Values

Wall Type	% Invulnerable Area (nominal), LA_roof	KE absorbed by wall (ft-lb) ΔKE_n
Steel Siding (22 Gauge)	2	1000
8 in. Unreinforced CMU (Concrete Masonry Unit)	2	500
8 in. Reinforced CMU	2	500
8 in. Reinforced Concrete	2	50000
14 in. Reinforced Concrete	2	200000
6 in. Reinforced Concrete Tilt-Up	2	37500
1/2 in. Plywood Siding	2	100
8 in. Unreinforced Brick	2	10000
Steel (automobile doors)	4	1000

146. Note that Tables 9 and 10 were calculated based on explosive fragments. While the DOD Explosives Safety Board values are based on penetrating projectiles, there was no data provided in the source document of these tables to provide the size, shape, or weight of the projectiles used to generate this data. In addition, there was no description of the process or parameters used to test these shelter materials.

147. Further research located a related report that contained the same kinetic energy absorption values (reference 11). In addition, this document SPIDER 2 TESTS – Response of Typical Wall Panels to Debris and Fragment Impact, contains details on the test methodology used to construct the absorption values. The report used an array of discarding sabot rounds with multiple cross sections to impact the wall and roof materials with calibrated energy levels. Figure 34 shows the sabot rounds used for the tests.

Figure 34: Projectiles Used for Impact Testing

148. Table 11 provides the type and size of materials used in the tests. For the purposes of this effort, the impact diameters were averaged and then a cross sectional area of 0.054 ft^2 was calculated as a cross sectional area scalar.

Table 11: Type and Size of Materials Used for Impact Testing

Impactor	Material	Impactor Diameter (in.)	Impactor Weight (lb)	Impactor Diameter (mm)	Impactor Weight (kg)
C1	Concrete	2.25	0.51	57.15	0.23
C2	Concrete	3	1.15	76.2	0.52
C3	Concrete	3.75	2.2	95.25	1
C4	Concrete	5	5.75	127	2.61
C5	Concrete	7.4	17.4	187.96	7.89
S1	Steel	1.125	0.2	28.575	0.09
S2	Steel	1.5	0.5	38.1	0.23
S3	Steel	1.875	1	47.625	0.45
S4	Steel	2.5	2.298	63.5	1.042

149. To determine the total amount of kinetic energy absorbed, one takes the cross-sectional area of the aircraft's fuselage and divides by the constant scalar above. This value is then multiplied by the kinetic energy absorption value from Tables 8 and 9 to determine the total kinetic energy absorbed by the shelter material.

150. While these results seem to validate the smaller cases of aircraft (i.e., those whose fuselage sections are within an order of magnitude of the base scalar value), there is concern that the assumption of a single scalar absorption factor may not be accurate when scaled to larger aircraft.

SHELTER CASE STUDIES

151. To counter this concern, three case studies of aircraft impacting different structures were examined. Using the same logic used for a 2x4 wood beam, the impact and absorption energies were calculated to compare against the real-life results provided in the accident investigation reports.

Aircraft	Robinson R44	Piper PA-28-236	Cirrus Design SR 20
Accident No.	NTSB CHI08FA293	NTSB CEN10FA124	AAB DCA07MA003
GW (lb)	2,500	2,150	3,050
Alternate Weight	1	75	189
Cruise Speed (kt)	110	108	155
Max Speed (kt)	130	123	N/A
Assumed Speed	110	123	140
Kinetic Energy (KE) (ft-lb)	134,000	50,192	163,862
Collision Building	Residential Home 	Office Building 	Brick Skyscraper 
Building Collision Type	Plywood Panelized	8 in. Reinforced Concrete	14 in. Reinforce Concrete
Roof or Wall	Roof	Wall	Wall
KE Absorption	33000	50000	200000
Residual KE	1300000	192	-36138
Lethal Limit (ft-lb)	55		
Fatal/Non-Fatal	Fatal	Fatal	Nonfatal
Actual Events			
Passengers/Crews	2 Fatalities	1 Fatality	2 Fatalities
Third Party Ground	No Injuries	1 Fatality;1 Serious Injured	Minor Injuries on Ground (Debris)

152. The first incident investigated is that of a Robinson R44 helicopter that collided with a residential home. The vehicle hit the roof of the house, proceeded to go through the top floor, destroyed most of the interior walls, exited the house out the first floor front door, and continued skidding 80 ft across the street into a neighbor's yard where it subsequently burst into flames. While the accident investigators could not conclude a speed at which the helicopter impacted the building, the air vehicle crashed into the home at night after transiting from a casino where, according to reports, the pilot had consumed some alcoholic beverages. Given the lack of any information that suggests the pilot attempted a recovery to avoid the house, the assumption is made that the pilot conducted what is known as CFIT. The pilot lost his spatial awareness, which prevented him from maintaining proper altitude minimums. As expected from the pre-impact and absorption kinetic energies, the roof was not sufficient to prevent the air vehicle from entering

the house. The pilot, and his passenger, died from the impacts with the ground. The family suffered no injuries, but could have easily been killed had the crash occurred at a different angle. The impacted house can be seen in Figure 35.

Figure 35: Residential House Impacted by Helicopter

153. The second incident evaluated is that of an intentional flight into an Austin Internal Revenue Service (IRS) building. A software developer, reportedly overcome with economic and social grief, piloted his Piper Cub general aviation aircraft into the IRS building. For calculating the kinetic energy prior to impact, it was assumed that the pilot flew the aircraft at its maximum velocity rather than the cruise velocity. This is based on the intent to do harm to the building and any personnel inside. This is particularly important for this case, as the cruise velocity would have resulted in a kinetic energy less than that for the value that could be absorbed by the building. At a faster velocity, 135 kt, however, the aircraft would impact the building and continue through the exterior walls with enough kinetic energy remaining to kill someone inside. In addition to the high velocity impact, the air vehicle set fire to the interior of the building. The fire spread throughout the building as seen in the image above and caused extensive damage greatly in excess of the initial aircraft impact. It is examples like this, and the combustive capability of many commercial related products (ex. Office furniture, carpets, paint), that the effects of secondary fires are not reduced due to shelter. These secondary fire effects will be discussed further in a following section. Figure 36 shows the building struck by the aircraft.

Figure 36: IRS Building Struck by Piper Cub

154. The third and final investigation was conducted from an accident in New York City. A pilot was at the controls of his Cirrus general aviation airplane with an instructor pilot monitoring the flight. After flying around the statue of liberty, the aircraft was piloted up the East River (Point E on Figure 37). The pilot, possibly attempting to avoid heading into class B airspace that began at the connection of the East Channel and East River, attempted to perform a 180 deg turn. Accident investigation details show that the wind was in the direction of the turn, the aircraft did not make the maximum use out of the space provided, and witness accounts suggest the aircraft was not turning at its maximum rate. Whatever the pilot's logic in the turn was, the airplane impacted a 520 ft apartment building, approximately 333 ft above street level. Figure 38 shows another view of the accident scene.

Figure 37: Flight Path of Cirrus

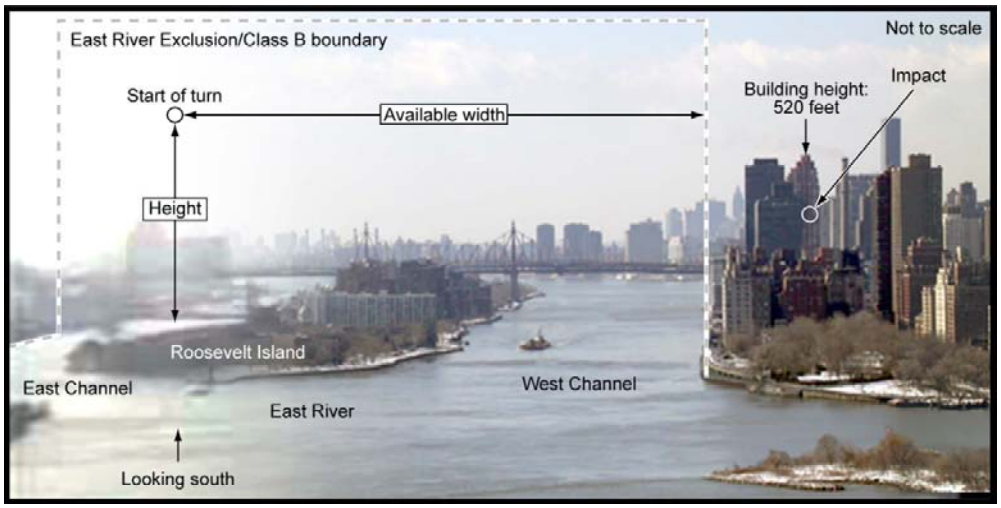

Figure 38: View of Available Turn Space

155. While the pilot and instructor were killed, there was no loss of life from within the interior of the building. This report confirms the calculated results that suggest that this collision would be non-fatal to individuals inside the shelter. It should be pointed out that injuries were sustained from individuals on the ground exterior of the building as a result of falling debris.

STANDARD U.S. SHELTER SIZES

Model for Rural Shelter

156. For the rural shelter area, the assumption was made that the majority of structures in rural and other non-Urban environments would primarily be residential homes. According to the National Association of Home Builders, the average home size in the U.S. was 2,700 ft^2 in 2009 (reference 15). Dividing the mean square footage to a single story results in a conservative assumption in order to give the maximum total area in which an aircraft could impact. The dimensions of the building were then assumed to be square to represent approximately the same susceptibility to aircraft impact on each side.[14] The height is assumed to be 15 ft, with 10 ft for the single floor and 5 ft for the roof. Glass percentage of the exterior walls is estimated at 10%. Following most common home materials, plywood panelized construction and ½ in. Plywood siding are assumed to be the construction of the roof and walls, respectively.

[14]A circle was considered as it would present the most accurate representation of a target area that had purely the same probability of impact from every angle. Given the extremely small number of circular buildings (limited to some stadiums and arenas) there was concern that this representation would not be keeping with traditional building construction and that a square was did not drastically reduce the orientation concerns.

Model for Urban Shelter

157. In order to model shelter for an urban environment, the team required data on buildings common to urban areas. Commercial buildings that include everything from universities, hospitals, office buildings, and others could be considered adequate examples of urban shelter. A 2003 Commercial Buildings Energy Consumption Survey done for the Energy Information Administration estimates that there were 4.9 million commercial buildings and more than 71.6 billion square feet of commercial floor space in the U.S. in 2003[15]. In addition to this information, the survey provided the number of buildings, total floor space, and mean square feet per building subdivided into the principal building activities (ex., Education, Food Sales, Food Service, Health Care, etc.). The survey then breaks apart the total buildings and floor space by region. The mean square feet per building was reported as 14,700. This is the area, assuming a single floor, used in this model as a baseline for urban shelter.[16]. Dividing the mean square footage to a single storey results in a conservative assumption in order to give the maximum total area in which an aircraft could impact. The dimensions of the building were then assumed to be square to represent approximately the same susceptibility to aircraft impact on each side. While the height of a single story is commonly referred to as 10 ft, the value of 20 ft will be used for the height as suggested by the DOD Explosive Safety Board. Additionally, the glass percentage of the building walls for an urban environment is assumed to be 25%. Building materials are assumed to be 4 in. reinforced concrete roofs and 6 in. reinforced concrete tilt-up walls based on the Explosive Safety Board reports.

[15]The information provided in the CBECS data is not current. The report is supposed to be quadrennial, however, in 2007, the contractor EIA hired to report CBECS data provided data that EIA concluded did not meet the appropriate standards for quality or credible energy information. The 2011 report has been delayed and is in danger of being dropped completely due to agency budget cuts. The researchers contacted EIA researchers to determine if any of the 2007 data may be acceptable for, at a minimum, updating the 2003 results. Thomas Leckey responded via email that this was not possible and that he hopes to receive funding to complete a 2011 survey later this year. He also suggested the researchers investigate the DOE Buildings Energy Data Book for information. While the Buildings Energy Data Book was insufficient for the purpose of determining building size, the resource would be useful elsewhere. The CBECS website along with contact information may be found here http://www.eia.gov/emeu/cbecs/.

[16]According to the Buildings Energy Data Book published by the Department of Energy, single story commercial buildings account for 40% in the U.S., with two stories accounting for 25%, and three story for 12%. Buildings between four and nine stories accounts for a further 16% of the building types in U.S. Therefore, 92% of all commercial sector buildings are nine stories or less. For the purposes of this effort, the choice was made to model the urban shelter off of a single story.

BLAST INDUCED EFFECTS

EQUIVALENT TNT

158. Given the right circumstances, an aircraft may explode upon impact with the ground due to the ignition of fuel vapors within the aircraft. As a result, an appropriate model for the effects of explosions must be created. While many sources can describe ways of calculating these effects, they do so based on an effective yield of TNT. Therefore, the first step of this process should be determining a relationship between equivalents weight of TNT and aviation fuel.

159. Technically speaking, a fuel air explosion such as would be experienced with jet fuels, diesel fuel, and gasoline are considered deflagrations. Explosions by definition exhibit supersonic expansion of gasses. In a deflagration, the reaction releases gasses limited to subsonic expansion. This subsonic expansion generally results in lower overpressure and impulse values. It must be noted, however, that the energy density stored in fuels is much higher than that of explosives. If the right mixture of fuel vapor and air can be attained, then a tremendous deflagration release with large amounts of energy can be obtained. This is the principle behind such munitions as the BLU-82 “Daisy Cutter” and GBU-43/B Massive Ordnance Air Blast.

160. The Department of Commerce developed a model for analyzing the risk associated with fuel tanks and their proximity to nuclear power plants. The scenario assumes a tank of fuel with the entire non-liquid volume consisting of the optimal fuel air mixture for deflagration. The governing equations involve the use of the ideal gas law that relates pressure, temperature, and volume to the amount of substance confined in the tank. The volume of the tank does not include any liquid volume in the tank. This is only the volume in which the fuel is in vapor (gaseous) form. The ideal gas law is given by equation 48.

$$n_{tot} = \frac{P\,V_{Tank}}{R\,T_{Flash}} \qquad (48)$$

Where:

N_{tot} = Moles of gas vapor in the tank
P = Pressure
T_{flash} = Flash point temperature of the fuel air mixture (in degrees rankine)
R = Gas constant
V_{tank} = Volume of the tank (gas volume only)

161. The total mass of the fuel vapor within a tank can be calculate based on the total amount of material in moles, the concentration of the fuel vapor and the molecular weight of the fuel. The concentration of the fuel vapor is assumed the upper flammable limit. This is the concentration at which anything above will prove the fuel air mixture to be too rich to ignite, however, the higher concentration provides the upper level of equivalent TNT while remaining within ignition limits. This is a conservative assumption. The molecular weights of the different fuels were found in Table 12. Equation 49 can be used to find the total vapor mass of fuel within the tanks.

Table 12: Characteristics of Select Aviation Fuels

Fuel	JP-4	JP-5	JP-8	Diesel
Molecular Weight (g/mol)	123	172	163	170
Fuel Flash Point (°F)	10	140	115	140
Fuel Flash Point (°R)	469.67	599.67	574.67	599.67
Heat of Combustion (MJ/Kg,min)	42.8	42.6	42.8	44.4
Fuel (LEL)	0.9	0.7	0.7	0.7
Fuel Concentration (UEL)	8	5	5	7
Explosion Efficiency High (%)	3	3	3	3
Explosion Efficiency Low (%)	8	5	5	5
Explosion Limit (%)	100	100	100	100
Heat of Combustion (BTU/lb)	18400.69	18314.7	18400.69	19088.56

$$M = cn_{tot}mw \qquad (49)$$

Where:
M = Mass of fuel vapor
c = Conversion constant (grams/lb)
n_{tot} = Total moles of vapor
mw = Molecular weight of fuel vapor

162. Once the total mass of the fuel in vapor phase has been calculated, the equivalent weight of TNT can be determined. The heat of combustion for the fuels E_{Fuel}, is also provided in Table 12. The heat of combustion, E_{TNT}, of TNT is 1943 BTU/lb. Finally, equation 50 can be used to determine the equivalent weight of TNT. The value of η is the efficiency of explosions. For completeness, three cases are assumed: a sensitivity case, a parametric case (5%), and a boundary value (100%). While the 100% factor would be most conservative, it is not practical to determine lethality. Instead, the 5% case is used for this effort (reference 14).

$$W_{Equivalent} = \frac{\eta M E_{Fuel}}{E_{TNT}} \qquad (50)$$

BLAST IMPULSE AREA

163. This section deals specifically with thermal radiation as a direct result of deflagration type explosions. Details on the lethal area of secondary fuel fires are provided in the following section. Detonations of explosives are identified by supersonic shock waves carrying large pressure differences. These pressure waves move away from the source explosion at supersonic speeds. This type of explosion would be reminiscent of munitions exploding. This is not the focus of this effort and will not be discussed. Instead, the danger of deflagration due to unspent or undumped fuel will be examined. This type of detonation is defined as a rapid, yet subsonic, expansion of gases burning at high temperature.

164. The effects of blast pressure and impulse can have significant effects on the human body. A large pressure differential across a person's body will result in a rapid movement of air in and out of the lungs through all available orifices. The rapid contracting and expansion of the lungs, because of the pressure differential, will cause lung rupture, and if not treated rapidly, eventual death. Similarly, the impulse from the pressure wave can knock an individual over, throw the individual, or cause passive objects to turn into projectiles that may cause bodily harm.

165. The goal of this section is to calculate the distance from the center of the detonation that represents the lethal area around the air vehicle. The first step is to calculate the hazard factor Z. From equation 51, this can be calculated first by the distance, D, from the center of the explosion and the equivalent weight, W, of TNT as calculated above (reference 14).

$$Z = \frac{D}{W^{1/3}} \qquad (51)$$

166. The unmodified pressure of the detonation can then be calculated using a process defined by the DOD's approved algorithms' for explosive safety analysis. A logarithmic curve fit was created based on explosives testing. First, a value of x is determined from Z using equation 52

$$x = LN(Z) \qquad (52)$$

The unmodified pressure can then be calculated using the exponential function in equation 53 where the coefficients for the function are provided in Table 13 and are dependent of the range of Z.

$$P_o = e^{(A+Bx+Cx^2+Dx^3+Ex^4)} \qquad (53)$$

Table 13: Unmodified Pressure Coefficients

Z Range (ft-lb^1/3)	A	B	C	D	E
0-7.25	6.9137	-1.4398	-0.2815	-0.1416	0.0685
7.25-60	8.8035	-3.7001	0.2709	0.0733	-0.0127
60-500	5.4233	-1.4006	0	0	0

167. Similarly, the unmodified impulse is modeled using equation 54. Note that the additional Y term that represents the yield of the detonation. For this analysis, it is assumed that Y = W. This is often not the case for explosives, but will suffice for a fuel air deflagration. The Unmodified Impulse coefficients for equation 54 are available in table 14.

$$I_o = e^{(A+Bx+Cx^2+Dx^3+Ex^4)} Y^{\frac{1}{3}} \qquad (54)$$

Table 14: Unmodified Impulse Coefficients

Z Range (ft-lb^1/3)	A	B	C	D	E
0-2.41	2.975	-0.466	0.963	0.03	-0.087
2.41-6	0.911	7.26	-7.459	2.96	-0.432
6-85	3.2484	0.1633	-0.4416	0.0793	-0.00554
85-400	4.7702	-1.062	0	0	0

168. The effects of shelter can reduce the impact that an overpressure will have on lethality limits. The Vent Area to Volume Ratio (VAVR) represents the area within a shelter that will allow the release of overpressures. This value is a function of the floor area, A_{Floor} the Glass percentage of the shelter,G_P and the Height of the shelter, $H_{Shelter}$. Typical shelter heights are provided in Table 15.

$$\mathrm{VAVR} = \frac{2.5+\mathrm{G_P}}{100}\frac{1}{\mathrm{A_{Floor}}\times\mathrm{H_{Shelter}}} \qquad (55)$$

Table 15: Typical Shelter Heights

Shelter	Height (ft)
Vehicle	4
Trailer/Modular Building	10
Wood Frame/Steel Stud/Masonry/Concrete	12
Large Reinforced Concrete Tilt-up	20
Large PEMB (Office/Storage/Hangar)	24

169. Next, a reduction value (RV) can be calculated. This reduction value can be calculated from the unmodified pressure and the equivalent weight. The equation used depends on the vent area ratio determined above. If the vent area is greater than 0.005, then equation 56 is used, else equation 57 is used.

$$\mathrm{RV_{vent|VAVR>0.005}} = 0.3\ \mathrm{W_a^{0.095}P_O^{-0.32}} \qquad (56)$$

$$\mathrm{RV_{vent|VAVR<0.005}} = 0.3\ \mathrm{W_a^{0.095}P_O^{-0.31}}[(0.392 + 0.0568 * \mathrm{Log10(P_o)}] \qquad (57)$$

170. The purpose of these two equations is to determine the average reduction value for venting. Based on Glass fraction and equation 58, it can be seen that the Reduction Level (RL) of overpressure is a function of glass percentage for a given reduction value. The RL can be approximated using a stepwise function where the reduction value is 0.5 for glass fractions less than 7.5%, equal to equation 58 for values between 7.5% and 25% glass fraction, and 0 for all glass fraction values above 25%.

$$\mathrm{RL} = \left(\mathrm{slope} \times \frac{\mathrm{Gp}}{100}\right) + \mathrm{b_{intercept}} \qquad (58)$$

171. Incorporating the reduction level to the unmodified blast pressure and impulse already calculated results in the final pressure and impulse felt inside a shelter or P_{Final} and I_{Final}, respectively.

$$\mathrm{P_{Final}} = (1 - \mathrm{RL})\mathrm{P_o} \qquad (59)$$

$$\mathrm{I_{Final}} = (1 - \mathrm{RL})\mathrm{I_o} \qquad (60)$$

172. Now that the final pressure and impulse from the detonation have been determined, the values of pressure and impulse directly related to lethality can be examined. For this analysis, it is assumed that the ambient pressure, $P_{ambient}$, is equal to 14.5 psi. The reflected pressure can be determined through equation 61.

$$\mathrm{P_{reflected}} = 2\mathrm{P_{Final}}\left(\frac{4\mathrm{P_{Final}}+7\mathrm{P_{ambient}}}{\mathrm{P_{Final}}+7\mathrm{P_{ambient}}}\right) \qquad (61)$$

173. Likewise, the dynamic pressure can be calculated using equation 62.

$$\mathrm{P_{dynamic}} = \frac{2.5\times\mathrm{P_{final}^3}}{7\times\mathrm{P_{ambient}}+\mathrm{P_{Final}}} \qquad (62)$$

174. The case of calculating the nominal pressure depends on whether a shelter is available. For cases of shelter, the nominal pressure is simply the reflected pressure. When there is no pressure, the nominal pressure can be determined from equation 63.

$$\mathrm{P_{nom}} = \mathrm{P_{Final}} + \mathrm{P_{dynamic}} \qquad (63)$$

175. The scaled pressure is a function of both the dynamic pressure calculated in equation 62 and the assumed ambient pressure or 14.5 psi. The values shown are used to convert the imperial units used throughout this assessment to metric units that are used for the lethality model. This is shown in equation 64.

$$\mathrm{P_{scaled}} = \frac{6.895\times\mathrm{P_{dynamic}}}{0.001\times\mathrm{P_{ambient}}} \qquad (64)$$

176. Similarly, unit conversion is used to determine the scaled impulse in equation 65.

$$\mathrm{I_{Scale}} = 0.005291 \times \mathrm{I_{Shelter}} \qquad (65)$$

177. The values of pressure and impulse are used in equations developed by and used by the DOD Explosives Safety Board to determine the probability of lethality due to the three causes associated with blast impulse results; lung rupture, body displacement, and skull fracture (reference 14).

178. For lung rupture, the probability function shown in equation 66 is a function of scaled pressure and impulse.

$$s_{\text{Lung Rupture}} = \frac{4.2}{P_{\text{scaled}}} + \frac{1.3}{I_{\text{Scale}}} \qquad (66)$$

179. A normal probability distribution is then defined as a function of the s value. This determines the probability of lethality dependent on all the functions previously stated. Different numerical methods including, but not limited to, excel's goal seek function may be used to determine the radius of lethality from the probability of lethality.

$$z_{Lung\ Rupter} = -5.74LN(s_{Lung\ Rupture}) \qquad (67)$$

180. In similar fashion, the probability function and z values for body displacement can be calculated using equations 68 and 69.

$$s_{\text{Body Displacement}} = \frac{7280}{6895 \times P_{\text{nom}}} + \frac{1.3 \times 10^9}{6895 \times P_{\text{nom}} \times I_{\text{Scale}} \times 6.895} \qquad (68)$$

$$z_{\text{Body Displacement}} = -2.444\text{LN}(s_{\text{Body Displacement}}) \qquad (69)$$

181. Note that these set of equations depend on the nominal pressure and scaled impulse. Once the probability is known, the radius of fatality due to body displacement is calculated assuming a 10% lethality threshold.

182. Finally, the values of lethality due to skull fracture can be determined. Note that the likelihood of skull fracture is a conservative assumption. One must assume that there are materials available in and around the detonation area. The resultant function and distribution function are provided in equations 70 and 71.

$$s_{\text{Skull Fracture}} = \frac{2430}{6895 \times P_{\text{nom}}} + \frac{4 \times 10^9}{6895 \times P_{\text{nom}} \times I_{\text{Scale}} \times 6.895} \qquad (70)$$

$$z_{\text{Skull Fracture}} = -8.49 \times \text{LN}(s_{\text{Skull Fracture}}) \qquad (71)$$

183. Using the same process of solving backward for distance from the detonation site, the lethal area may be calculated assuming a probability of lethality of 10%.

THERMAL RADIATION AND BURN AREA

184. This section deals specifically with thermal radiation as a direct result of deflagration type explosions. A part of this step is to look at the lethal area or range due solely to thermal radiation from the deflagration. As part of the analysis, the same hazard factor from the previous section will be used. Where D is the distance from the detonation and W is the equivalent weight of TNT of the fuel vapor air mass previously defined and calculated above.

$$Z = \frac{D}{W^{1/3}} \qquad (72)$$

185. Once this equivalent weight of TNT has been established, the results can be incorporated into the model used by the DOD for explosives safety analysis for thermal effects. After calculating the value for Z, the affect of shelter can be included. The thermal blocking factor, TBF, can be calculated using equation 73:

$$\mathrm{TBF} = \mathrm{TBF_o}\frac{100-\mathrm{G_P}}{\mathrm{G_P}} \qquad (73)$$

186. Where G_P is the Glass Percentage of the shelter and TBF_o is the nominal thermal blocking factor for a given structure. The nominal values for TBF_o for selected building materials and floor area are provided in Table 16.

Table 16: Nominal Thermal Blocking Factors

Shelter	Nominal Thermal Blocking Factor
Small reinforced concrete (< 5,000 ft^2)	1
Medium reinforced concrete (5,000-20,000 ft^2)	1
Large tilt-up reinforced concrete (> 20,000 ft^2)	1
Small reinforced masonry (< 5,000 ft^2)	1
Medium reinforced masonry (5,000-20,000 ft^2)	1
Small unreinforced brick (< 5,000 ft^2)	1
Medium unreinforced masonry (5,000-20,000 ft^2)	1
Large unreinforced masonry (> 20,000 ft^2)	1
Small PEMB (< 5,000 ft^2)	0.2
Medium PEMB (5,000-20,000 ft^2)	0.2
Large PEMB (> 20,000 ft^2)	0.2
Small wood frame (< 5,000 ft^2)	0.2
Medium wood frame (5,000-20,000 ft^2)	0.2
Medium steel stud (5,000-20,000 ft^2)	0.2
Wood frame(~500 ft^2)	0.2
Moving vehicle	0.6
Stationary vehicle	0.6

187. The probability of lethality can be calculated using equation 74 derived in the DOD risk analysis program.

$$P_{Lethality\_Thermal} = \frac{0.000232263}{0.00005493+e^{\frac{-14.8}{Z}}} \qquad (74)$$

188. The reduction in lethality due to shelter can be incorporated by using the resultant TBF and equation 75.

$$P_{Lethality\_Thermal|Shelter} = (1 - TBF) * P_{Lethality\_Thermal} \qquad (75)$$

189. In order to determine the lethal area, a probability of lethality of 10% is assumed and the radius may be back solved from this result. Note that the 10% is the same value as used by the skull fracture lethality model described earlier.

190. In addition to the direct thermal effects, the safety paper suggests that any individual within range of the fireball radius, R_{FB}, would be considered as a fatality (reference 14). Therefore, a model for the radius must be assumed. Equation 76 is used by the DOD Explosives Safety analysis. This is the same value used in the skull fracture lethality curve.

$$R_{FB} = 2.77 \frac{W}{0.45}^{0.36} \qquad (76)$$

191. A separate model was used to compare fireball radius size. Using a fireball radius described in Lee's Loss Prevention in the Process Industries, a similar size of resultant fireball radius was calculated (reference 26). The Lee model was consistently below that of the DOD Risk analysis model. Therefore, the assumption was made to use the fireball radius provided in the DOD approach as the more conservative option.

SECONDARY FIRES

192. Fires due to unspent or undumped fuel represent a significant hazard to personnel on the ground. An intense fire may quickly spread into a conflagration and start ingesting shelter and other combustible materials. This method does not investigate the affects of fire spreading from the crash site; however, it does seek to determine the lethal area as a result of a secondary fuel fire and suggest some methods of integrating shelter affects into the model (reference 27).

193. The first step in determining the total lethal area surrounding a fire is to determine the area of which the fuel will cover. The simplest method of estimating the diameter of an unconfined fuel spill is shown in equation 77.

$$D = 10\sqrt{V} \qquad (77)$$

Where:
D = Diameter of spill
V = Volume of fuel spilled

194. Next, the heat release rate of the fire is calculated by multiplying the area of the fuel spill by the thermal flux of a given fuel. The value of thermal flux is found by multiplying the mass rate of fuel burn by the heat of combustion. This information is available for selected fuels in Figure 17.

Table 17: Mass Burning Rate, Heat of Combustion, and Thermal Flux for Select Fuels

Liquid	Mass Burning Rate, m_dot kg/m^2*1/s	Heat of Combustion kJ/kg	Thermal Flux kW/m^2
Acetic Acid	0.033	13,100	400
Acetone	0.041	25,800	1,100
Acrylonitrile	0.052	31,900	1,700
Amyl Acetate	0.102	32,400	3,300
Amyl Alcohol	0.069	34,500	2,400
Benzene	0.048	44,700	2,100
Butyl Acetate	0.1	37,700	3,800
Butyl Alcohol	0.054	35,900	1,900
m-Cresol	0.082	32,600	2,700
Crude Oil	0.045	42,600	1,900
Cumene	0.132	41,200	5,400
Cyclohexane	0.122	43,500	5,300
No. 2 Diesel Fuel	0.035	39,700	1,400
Ethyl Acetate	0.064	23,400	1,500
Ethyl Acrylate	0.089	25,700	2,300
Ethyl Alcohol	0.015	26,800	400
Ethyl Benzene	0.121	40,900	4,900
Ethyl Ether	0.094	33,800	3,200
Gasoline	0.055	43,700	2,400
Hexane	0.074	44,700	3,300
Heptane	0.101	44,600	4,500
Isobutyl Alcohol	0.054	35,900	1,900
Isopropyl Acetate	0.073	27,200	2,000
Isopropyl Alcohol	0.046	30,500	1,400
JP-4	0.051	43,500	2,200
JP-5	0.054	43,000	2,300
Kerosene	0.039	43,200	1,700
Methyl Alcohol	0.017	20,000	340
Methyl Ethyl Ketone	0.072	31,500	2,300
Pentane	0.126	45,000	5,700
Toluene	0.112	40,500	4,500
Vinyl Acetate	0.136	22,700	3,100
Xylene	0.09	40,800	3,700

195. The thermal area covered by a spill is given by equation 78 and the total thermal energy generated is the thermal flux multiplied by this area which can be found in equation 79.

$$A = \pi \left(\frac{D}{2}\right)^2 \qquad (78)$$

$$\dot{Q} = A \times \dot{q}_{fuel} \qquad (79)$$

196. Assuming the energy release of the fuel can be estimated as a point source, the resulting equation can be used. The value of $\dot{q}''$ is the amount of heat flux at a distance r from the fire's center.

$$\dot{q}'' = \frac{\chi_r \dot{Q}}{4\pi r^2} \qquad (80)$$

197. From experimental results, the value of χ_r can be determined as

$$\chi_r = \chi_{r_{max}} e^{-kD} \qquad (81)$$

198. Where $\chi_{r_{max}}$ is 0.34 and k is 0.05 1/m. To determine the lethal area, the lethal amount of heat influx should be inserted and the equation simplified for the value of r. According to published requirements, the maximum $\dot{q}''$ for people is 1.4 kW/m^2. While this may be a reasonable threshold for injury, it is too conservative for lethality.

199. A study in the New England Journal of Medicine determined the probability of lethality was closely related to three factors; age over 60, smoke inhalation, and burns to >40% of the body (reference 10). The data from this table is shown in Table 18.

Table 18: Actual/Estimated Mortality Due to Fire

No. of Risk Factors	No. of Patients	No. of Deaths	Estimated No. of Deaths	Actual Mortality	Estimated Mortality (90% CI)*
				percent	
0	1314	3	3	0.2	0.3 (0.1–0.6)
1	218	10	8	5	3 (2–5)
2	111	33	37	30	33 (26–41)
3	22	21	19	95	87 (78–93)

*CI denotes confidence interval.

200. This effort makes several key assumptions to use this result, with the high confidence data results, to link lethality to fire. The first is that if a person receives enough heat to be receiving burns, they will experience smoke inhalation. In a crash smoke movement will be dependent on several factors so for simplicity the assumption is made that if burning occurs due to an aircraft crash, there is most likely smoke inhalation. The second assumption is that the affects of fire to the general population will be the same as that of a 60 year old or greater. This is a conservative assumption in order to reduce the lethality to a single factor, percentage of burned flesh. It will be assumed that burning of flesh must occur on greater than 40% of the bodies' surface. For an approximation, if the burns were suffered on half of the representative man cylinders, then one could anticipate a likelihood of lethality.

201. The journal article does not refer to the temperatures required to cause skin burns. Other sources including Lawrence (reference 22) and Ng (reference 30) revealed that several tests were conducted on animals and cadavers which determined that flesh will begin burning within 10 sec at temperatures between 60°C and 70°C. Defining the ambient temperature of the skin surface to be 37°C (98.6°F), 23°C of temperature change of the epidermis is required to cause burning. The coefficient of heat for the human epidermis is defined to be 3598 J/kg-K and the weight of half

the human skin is 5.6 kg [17]. The resulting minimum heat flux for lethality, $\dot{q}''_{lethal}$, is 15.44 kW/m^2. At this rate, pain would be felt in under 10 sec and 2nd degree burns in 30 sec. This would suggest that if the reference person cannot distance themselves within 3-5 min, there is a likelihood of lethality.

202. Thus, the radius is given by equation 82.

$$r = \sqrt{\frac{\chi_r \times \dot{Q}}{4\pi \dot{q}''_{lethal}}} = \sqrt{\frac{\chi_r \times \pi\left(\frac{D}{2}\right)^2 \times \dot{q}_{fuel}}{4\pi \dot{q}''_{lethal}}} = \sqrt{\frac{\chi_r \times \pi\left(\frac{10\sqrt{V}}{2}\right)^2 \times \dot{q}_{fuel}}{4\pi \dot{q}''_{lethal}}} \qquad (82)$$

203. In addition, the lethal area can be simplified to a function of the total amount of unspent fuel released from the aircraft.

$$AL_{\text{Secondary Fire}} = \pi r^2 = \pi\left(\frac{\chi_r \times \pi\left(\frac{10\sqrt{V}}{2}\right)^2 \times \dot{q}_{fuel}}{4\pi \dot{q}''_{lethal}}\right) \qquad (83)$$

TOOL IMPLEMENTATION

204. The models and methods provided in this report are currently being implemented into the 3rd Party Risk Assessment Tool (3PRAT). Due to the complexity of some of the methods and models, the tool is being built in stages to reflect updates, corrections, and streamlining to the overall model. A thorough description of the current model construction, implementation, and user manipulation is provided in a separate document, 3PRAT Guidebook.

205. It is recommended that further work be done to improve the effects of blast-impulse and research air-vehicle fragmentation for their affects on both lethality and the total crash area.

[17]The human skin is the largest organ of the body accounting for 16% of the body. The mass referenced here is the mass of our reference man multiplied by the amount of skin and divided by two to represent half of the skin.

THIS PAGE INTENTIONALLY LEFT BLANK

RESULTS

206. The tool implemented using the methods described in this report can be applied to a variety of UAS currently in the U.S. Government inventory. The LCA for both glide and dive approaches is evaluated and compared to determine if any trends emerge.

207. Ten UAS manufactured and/or operated by U.S. Government agencies are provided in Table 19. Included is their maximum takeoff weight, the maximum fuel load, the limiting speed on the aircraft, the service ceiling, and the primary aircraft dimension (wingspan for airplanes vice rotor diameter for helicopters). These parameters, along with several others, were entered into the 3PRAT. The LCA for both controlled flight termination, as well as departure or dive flight termination, are provided in Table 19.

Table 19: UAS Manufactured and/or Operated by U.S. Government Agencies

Designation	Max Gross Takeoff Weight (lb)	Fuel Load (lb)	Max Speed (kt)	Operating Altitude (ft AGL)	Wingspan/ Rotor Diameter (ft)	LCA (Glide) (ft^2)	LCA (Dive) (ft^2)
MQ-8B	3,150	1,275	125	20,000	27.5	N/A	2,316
MQ-4C	32,250	17,300	450	60,000	130.9	83,214	13,685
Integrator	135	41	80	15,000	16	1,620	227
RQ-7	375	120	118	15,000	14	1,636	192
Scan Eagle	39.7	9.5	75	16,000	10.2	811	98
RQ-1C	3,200	580	135	29,000	56	12,033	2,552
RQ-1	2,250	665	117	25,000	48.7	9,551	1,940
Fury 1500	300	114	116	15,000	14.3	1,606	184
RQ-11	4.2	0	52	1,000	4.6	199	25
Desert Hawk	7	0	49.5	1,000	4.3	183	22

CASE STUDIES – RE-AFFIRMING THE DANGERS OF SMALL UAS

TWO DETAILED CASES OF UAS CAUSING FATALITIES DUE TO FAILURE PLUS ADDITIONAL REPORTS

208. Remote controlled (RC) helicopters and aircraft are not scrutinized to the same level as their manned counterparts. The relative size and energy limits, in addition to cost compared to manned flight, results in a safer, but not completely risk free hobby for aviation enthusiasts. Two cases of unmanned RC aircraft causing fatalities are shown in the following paragraphs.

Rotary Wing

208. The first case is of an RC helicopter mishap in Houston, TX. The pilot lost control of the air vehicle for unknown reasons and the aircraft began approaching the pilot and an additional observer. News reports were unclear as to the actual events that happened; however, an RC helicopter enthusiast posting onto a blog provided additional details. He stated that the aircraft was a 60 size aircraft and that the pilot was demonstrating the aircraft for the victim. For unknown reasons (although postulated to be mechanical), the aircraft lurched toward the pilot and observer. The pilot evaded the aircraft and verbally warned the victim. The victim was unable to evade the aircraft, and the rotor blades struck the individual in the neck. The RC operations were conducted in a remote area outside Houston and thus required 35-40 min for paramedics to arrive. The victim did not survive.

209. Lacking details on the type of RC helicopter flown that day, parameters were used that would be consistent with a 60 size RC helicopter. The impact was the result of the rotor blades striking the victim. Therefore, the kinetic energy was defined as the total rotational kinetic energy for a typical 60 size RC helicopter. This resulted in a kinetic energy of 36 ft-lb. This would be considered as a non-fatal impact according to the crash lethality model previously suggested. That sustained energy is below the lethal limit for skull fracture, 15 ft-lb. This suggests that had the model not be combined into a single kinetic energy threshold, the 36 ft-lb from this aircraft could be considered enough to cause a lethal head injury.

Fixed Wing

210. The second example case is of an RC biplane in Budapest, Hungary, that lost control and flew into a crowd of spectators killing two individuals. The aircraft was flown by an experienced RC aircraft operator from Germany. He was conducting the flight as part of an air show event. Spectators were separated from the air operations by some distance. During the performance, the aircraft suddenly executed an uncommanded turn, continued to travel outside of the performance area, and approached the crowd. Later investigation revealed that radio interference from some other source lead to the loss of control.[18]. The aircraft crashed striking two people, a married couple, mortally wounding them.

211. The kinetic energy is based on both factual reporting and assumptions from individuals. Reports from the accident identify the biplane which could be used to determine the aircraft's parameters such as wingspan and weight. The velocity was not available in these reports. From RC aircraft blogs, an individual familiar with the operation of these types of aircraft described the velocity as approximately 60 mph based on observations of video recorded at the site. This video was available online; however, it has been since removed possibly due to sensitivity concerns. Using the "expert" testimony of a fellow RC enthusiast, the kinetic energy was calculated to be 601 ft-lb. This suggests that there was sufficient kinetic energy to kill two individual observers.

Aircraft	RC Helicopter	RC Biplane
Lethal Mechanism	Rotor Blades	Blunt Trauma
Fatalities	1	2
Aircraft Dimensions		
Wingspan/Rotor Radius (ft)	2.18	8.20
Weight/Rotor Weight (lbm or slugs)	0.01	1.55
Total Blade Moment of Inertia (Helo Only)	0.02	NA
Velocity (ft/s) / Rotation Speed (PRM)	1700	88
Kinetic Energy	36	601
Kinetic Energy Lethal Limit (ft-lb)	55	
Fatal/NonFatal	NonFatal	Fatal

[18]Germany enforces a frequency spectrum that allocates a specific bandwidth to RC aircraft. Hungary did not have the same level of scrutiny at the time of the accident and it is believed that some other device over powered the transmitter of the operator causing him to lose control.

Additional Small UAS Cases

212. In addition to these small UAS, there have been reports of additional incidents in which people have been killed due to small, seemingly safe UASs.

- 6 year old boy killed when model helicopter lost control and struck him in the head
- 5 year old girl killed when grandfather made mistake at controls
- 13 year old girl killed when model airplane struck her in the head
- 11 year old boy died when transmitter interference resulted in airplane loss of control
- Hang glider killed when RC glider contacted him (more than one instance of hang glider/RC mid-air collision)

213. These examples were not included due to the lack of detailed information to conduct a thorough analysis. They do show that the perceived risk to UAS should not be limited to larger tactical birds, but that even small UAS can inflict substantial damage.

CONCLUSIONS

214. This report discussed the modeling of Crash Lethality of UAS in support of the TLS effort currently being conducted by the U.S. Navy. The primary purpose of this document was to define the lethal areas as a result of a fixed wing or rotary wing UAS crashes. The risks identified for third party persons on the ground were identified as blunt trauma, blast impulse, fragmentation, thermal radiation, and the danger of secondary fires. Each risk identified was analyzed in an effort to develop a model for predicting the human tolerance for each risk and then determining the lethal limit. After evaluating both fixed wing and rotor wing aircraft, each risk category was evaluated for both of the two types of flight termination. As much as possible, the effects of shelter on the lethality levels were addressed. However, due to the limited scope of this effort, further work could be done in this regard. Further work into this area should focus on the thermal sheltering affects to secondary fires, the blunt trauma kinetic energy lethality as it relates to the lower limbs and greater scrutiny over the blast-impulse sections to ensure accuracy. All of the methods and processes outlined in this study will be implemented in developing the 3PRAT, which will be used to determine the lethal crash area of various UASs.

THIS PAGE INTENTIONALLY LEFT BLANK

REFERENCES

1. Anderson, John David. *Aircraft Performance and Design.* Boston: McGraw-Hill Companies, Inc., 1999.

2. Bechtel SAIC Compancy, LLC. *Industrial/Military Activity-Initiated Accident Screening Analysis.* s.l.: Bechtel SAIC Compancy, LLC, Jan 2008. Preclosure Safety Analysis Revision Document Identifier 000-PSA-MGR0-01500-000-00A.

3. Bhanu, Bir, et al. *A System for Obstacle Detection During Rotorcraft Low Altitude Flight.* 3, s.l.: IEEE Transactions on Aerospace and Electronic Systems, Jul 1996, Vol. 32. 0018-9251/96.

4. Bogosian, David and Avanessian, Hrire Der. *Blunt Trauma from Blast-Induced Building Debris.* San Antonio, Texas: K&C Paper P-04-01, Aug 2004. 31st Explosives Safety Seminar.

5. Bowen, I. G., et al. *Biophysical Mechanisms and Scaling Procedures Applicable in Assessing Responses of the Thorax Energized by Air-Blast Overpressures or by Non-Penetrating Missiles*. Albuquerque, NM: Lovelace Foundation for Medical Education and Research, Nov 1966. Technical Progress Report. Contract No. DA-49-146-XZ-372.

6. Burke, David. Small UAS Lethality Thresholds Based on Kinetic Energy – Draft, 2010.

7. Byrne, Jeffery, Cosgrove, Martin and Mehra, Raman. *Stereo Based Obstacle Detection for an Unmanned Air Vehicle.* Orlando, FL: IEEE International Conference on Robotics and Automation, May 2006. 0-7803-9505-0/06.

8. Clare, Victor R., et al. *Blunt Trauma Data Correlation.* Springfield, VA: National Technical Information Service: U.S. Department of Commerce, May 1974. EB-TR-75016.

9. Clothier, Reece, et al. *A Casualty Risk Analysis for Unmanned Aerial System (UAS) Operations over Inhabited Areas.* Queensland, Australia: Queensland University of Technology, 2007. AIAC12 - Twelfth Australian International Aerospace Congress, 2nd Australasian Unmanned Air Vehicles Conference, 19-22 Mar 2007. p. 15.

10. Colleen, Ryan. Schoenfeld, David. et al. *Objective Estimates of the Probability of Death from Burn Injuries*, New England Journal of Medicine. Massachusetts, Feb 1998.

11. Crull, Michelle. Tatom, John. Conway, Robert. *SPIDER 2 Tests- Response of Typical Wall Panels to Debris and Fragment Impact*, U.S. Army Engineering and Support Center. Huntsville, AL, Jul 2010.

12. Ford, Andrew T. and McEntee, Kevin J. *Assessment of the Risk to Ground Population Due to an Unmanned Aircraft In-Flight Failure.* Forth Worth TX: American Institute of Aeronautics and Astronautics, Inc., 13-15 Sep 2010. 10th AIAA Aviation Technology, Integration, and Operations (ATIO) Conference. p. 12.

13. Gollnick, Volker, Butter, Torsten and Reppelmund, Bernhard. *Helicopter Low Level Flight Using Trajectory Planning and Obstacle Avoidance* . s.l.: International Congress of the Aeronautical Sciences, 2006.

14. Hardwick, Meredith, et al. *Approved Methods and Algorithms for DOD Risk-Based Explosives Siting.* Alexandria, VA: Department of Defense Explosives Safety Board, 21 Jul 2009. DDESB Technical Paper 14, Rev. 4.

15. *Housing Data and Statistics* [http://www.nahb.org/page.aspx/landing/sectionID=113]

16. International Commission on Radiological Protection. *Report of the Task Group On Reference Man.* Oxford: Pergamon Press, 1975, Adopted Oct 1974.

17. Jan, Shau-Shiun and Lin, Yu-Hsiang. *Integrated Flight Path Planning System and Flight Control System for Unmanned Helicopters.* 11, s.l.: Sensors, 2011, Vol. 2011, pp. 7502-7529. ISSN 1424-8220.

18. Janser, Paul W. *Lethality of Unprotected Persons Due to Debris and Fragments.* Omni Hotel, Norfolk, VA, USA: Ernst Basler & Partners Consulting Engineers and Planners Zurich, Switzerland, 24-26 Aug 1982. Twentieth Explosives Safety Seminar. p. 16.

19. JHA, Shivendra, et al. *The pattern of fatal head injury in a teaching hospital in eastern Nepal.* 3, s.l.: Journal of Clinical and Diagnostic Research, Jun 2011, Vol. 5. 592-596.

20. Johnson, Wayne. *Helicopter Theory.* Princeton, New Jersey: Princeton University Press, 1994.

21. Kimura, Chris Y., et al. *Data Development Technical Support Document for the Aircraft Crash Risk Analysis Methodology (ACRAM) Standard.* Lawrence Livermore National Laboratory: United States Department of Energy, 1 Aug 1996. UCRL-ID-124837.

22. Lawrence, J.C. and Bull, J. P. *Thermal Conditions which Cause Skin Burns.* Volume 5 1976, Engineering in Medicine, pp. 61-63.

23. Leishman, J. Gordon. *Principles of Helicopter Aerodynamics.* New York, NY: Cambridge University Press, 2006.

24. Lyon, David H., Cynthia, Bir A and Patton, Bredan J. *Injury Evaluation Techniques for Non-Lethal Kinetic Energy Munitions.* Army research Laboratory. Aberdeen Proving Ground, MD: Department of Defense, Jan 1999. ARL-TR-1868.

25. Macqueen, Ainslie, Milborrow, Turner, Swift-Hook. *Risks Associated with Wind-Turbine Blade Failures.* IEE Proceedings, Vol. 130, pt. A, No. 9, Dec 1983.

26. Mannan, Sam. et al. *Lees' Loss Prevention in the Process Industries: Hazard Identification, Assessment and Control.,* 3rd Ed., Burlington, MA, 2005

27. McGrattan, Kevin B., Baum, Howard R. and Hamins, Anthony. *Thermal Radiation from Large Pool Fires.* Fire Safety Engineering Division. Building and Fire Research Laboratory: National Institute of Standards and Technology. Technology Administration. United States Department of Commerce, Nov 2000. NISTIR 6546.

28. Morgan, Colin. Bossanyi, Ervin. Siefert, Henry. *Assessment of Safety Risks Arising From Wind Turbine Icing.* Hetta, Finland. Apr 1998.

29. NASA, *Anthropometry and Biomechanics,* Volume I, Section 3. pp. 32-79 National Aeronautics and Space Administration. NASA-STD-3000 275

30. Ng, E Y-k and Chua, L T. *Prediction of Skin Burn Injury. Part 2: Parametric and Sensitivity Analysis,* 2002, Journal of Engineering in Medicine, Vol. 216.

31. Padfield and D., Gareth. Helicopter Flight Dynamics: The Theory and Application of Flying Qualities and Simulation Modeling. Oxford, UK: Blackwell Publishing Ltd., 1996.

32. Prouty, Raymond. *Helicopter Performance, Stability, and Control.* Malabar, FL: Krieger Publishing Company, Inc., 1986.

33. Raymer, Daniel P. *Aircraft Design: A Conceptual Approach.* Washington DC: American Institute of Aeronautics and Astronautics, Inc., 1992. ISBN 0-930403-51-7.

34. Raymond, David, et al. *Tolerance of the skull to blunt ballistic tempro-parietal impact.* Detroit, MI: Journal of Biomechanics, Jul 2009, Vol. 42, pp. 2479-2485. Doi: 10.1016.

35. Sanders-Reed, John N., et al. *Passive Obstacle Detection System (PODS) for Wire Detection.* San Diego, CA: SPIE, 2009. 7328.

36. Scherer, Sebastian, et al. *Flying Fast and Low Among Obstacles.* Roma, Italy: IEEE International Conference on Robotics and Automation, 10-14 Apr 2007. 1-4244-0602-1/07.

37. Shimo, Yoji. *Development of Power Transmission Line Inspection System by Unmanned Helicopter*. PARIS: CIGRE, 2006. B2/D2-106.

38. USDOE, Accident Analysis for Aircraft Crash into Hazardous Facilities. *DOE STANDARD: Accident Analysis for Aircraft Crash into Hazardous Facilities.* Washington DC: U.S. Department of Energy, May 2006. DOE-STD-3014-2006.

39. Zhou, Q., Rouhana, S.W. and Melvin, J.W. *Age Effects on Thoracic Injury Tolerance.* s.l.: Proceedings of the 40th Strapp Car Crash Conference, 4-6 Nov 1996.

DISTRIBUTION:

NAVAIRSYSCOM (AIR-4.3.1 - Cochran), Bldg. 2187, Room 3358 (4)
48110 Shaw Road, Patuxent River, MD 20670-1906
NAVAIRSYSCOM (AIR-4.5 - Burke), Bldg. 2272, Room 253 (5)
47123 Buse Road, Patuxent River, MD 20670-1547
NAVAIRSYSCOM (AIR-4.6.2 - Knott), Bldg. 2187, Room 1280D5 (2)
48110 Shaw Road, Patuxent River, MD 20670-1906
NAVAIRSYSCOM (AIR-4.5.1 - Andrew), Bldg. 2187, Room 2242 (2)
48110 Shaw Road, Patuxent River, MD 20670-1906
NAVAIRWARCENACDIV (5.1.2.1 - Ball), Bldg. 111, Room 240 (2)
22755 Saufley Road, Patuxent River, MD 20670-1619
U.S. Army Research Laboratory, (Bradley), Vehicle Technology Directorate (1)
4603 Flare Loop, Aberdeen Proving Grounds, MD 21005
NAVAIRWARCENACDIV (4.3.2.6 - Donley), Bldg. 2187, Room 1313 (1)
48110 Shaw Road, Patuxent River, MD 20670-1906
NAVAIRSYSCOM (AIR-4.10 - Polakovics), Bldg. 2187, (1)
48110 Shaw Road, Patuxent River, MD 20670-1906
NAVAIRWARCENACDIV (5.2.2G - Jacob), Bldg. 2118, Room 110 (1)
23013 Cedar Point Road, Patuxent River, MD 20670
NAVAIRSYSCOM (AIR-5.1G - Roberts), Bldg. 8010 (1)
47320 Priests Point Loop, St. Inigoes, MD 20684-4017
NAVAIRSYSCOM (UASTD - Heasley), Bldg. 8127 (1)
17637 Nesea Way, St. Inigoes, MD 20684-4015
NAVAIRSYSCOM (PEO U&W - Daniels), Bldg. 2272, Room 253 (1)
47123 Buse Road, Patuxent River, MD 20670-1547
NAVAIRSYSCOM (PEO U&W - Evans), Bldg. 2272, Room 246 (1)
47123 Buse Road, Patuxent River, MD 20670-1547
NAVAIRSYSCOM (AIR-4.1.6 - Zidzick), 235, Bldg. 4010, Room 235 (1)
48187 Standley Road, Patuxent River, MD 20670
NAVAIRSYSCOM (AIR-4.3D - Rubinsky), Bldg. 2187, Room 3322 (1)
48110 Shaw Road, Patuxent River, MD 20670-1906
NAVAIRSYSCOM (AIR-4.5.1 - Thorpe), Bldg. 2187, Room 2242 (1)
48110 Shaw Road, Patuxent River, MD 20670-1906
ARMY (RDMR-AEV - Flynn), 4488 Martin Road (1)
Redstone Arsenal, AL 35898
NAVAIRWARCENACDIV (AIR-4.0P - Adams), Bldg. 460, Room 222, (1)
22244 Cedar Point Road, Patuxent River, MD 20670-1163
NAVAIRDEVCENACDIV (AIR-5.0E - Rusher), Bldg. 1492, Room 24, (1)
47758 Ranch Road, Patuxent River, MD 20670-1456
WPAFB (ESC/ENSI - Rodreguez), Bldg. 28 (1)
Wright Patterson AFB, OH 45433
WPAFB (ABSSA/SIPT - Schaeffer), Area B, Bldg. 557, Room 005D (1)
Wright Patterson AFB, OH 45433

Pentagon (OUSD [AT&L]/S&TS-Unmanned Warfare - Greenly), Room 3B938 (1)
3090 Defense Pentagon, Washington, DC 20301-3090
NAVAIRWARCENACDIV (4.12.6.2), Bldg. 407, Room 116 (1)
22269 Cedar Point Road, Patuxent River, MD 20670-1120
DTIC (1)
8725 John J. Kingman Road, Suite 0944, Ft. Belvoir, VA 22060-6218

NAVAL AIR WARFARE CENTER AIRCRAFT DIVISION
PATUXENT RIVER, MARYLAND

ERRATA

ERRATA NUMBER: NAWCADPAX/RTR-2012/196E

DATE: 2 July 2013

FROM:
Commander, Naval Air Warfare Center Aircraft Division, Patuxent River, Maryland 20670-1161

TO:
Commander, Naval Air Systems Command Headquarters, 47123 Buse Road, Patuxent River, Maryland 20670-1547

REPORT NO.:	**DATE:**
NAWCADPAX/RTR-2012/196	6 June 2012

REPORT TITLE:
Crash Lethality Model

REQUEST THAT RECIPIENTS OF THE ABOVE REPORT INCORPORATE THE FOLLOWING CORRECTIONS:

Per Public Release Authorization Request No. 2013-591, make pen and ink change to Distribution statement to read:
Approved for public release; distribution is unlimited.

DISTRIBUTION:	**RELEASED BY:**
Same as original document.	27 Jun 2013 ROLAND COCHRAN / 4.3.1 / DATE Air Vehicle Systems Engineering Division Naval Air Warfare Center Aircraft Division

B3823378

2012084431

Approved for public release; distribution is unlimited.